JOURNAL OF MATERIALS SCIENCE 32 (1997) 893–911

A model SiC-based fibre with a low oxygen content prepared from a polycarbosilane precursor

G. CHOLLON, M. CZERNIAK, R. PAILLER, X. BOURRAT, R. NASLAIN
Laboratoire des Composites Thermostructuraux, UMR-47, 3 Allée de la Boetie, 33600 Pessac, France

J. P. PILLOT
Laboratoire de Chimie Organique et Organométallique URA-35, Université de Bordeaux-I, 351 Cours de la Libération, 33400 Talence, France

R. CANNET
Centre de Recherche Paul Pascal du CNRS, UPR-8641, Avenue A. Schweitzer, 33600 Pessac, France

A model SiC-fibre has been prepared from a polycarbosilane precursor by means of an irradiation oxygen-free curing process. The chemical composition remains unchanged after heat treatments under an inert atmosphere for pyrolysis temperatures of 1600 °C. At this temperature, the fibre consists of SiC nanocrystals (mean size 6–10 nm) and free carbon. However, a slow grain growth takes place as the temperature is increased. The fibre retains a high strength at room and high temperatures up to temperatures of 1600 °C when the pyrolysis has been performed under nitrogen. The electrical conductivity was studied as a function of the pyrolysis temperature T_p: For $1100 \leqslant T_p \leqslant 1200$ °C, the conductivity increases by several orders of magnitude due to the reorganization of the free carbon phase at the SiC grain boundaries. Oxidation kinetics of the filaments remain parabolic from 1000–1400 °C.

1. Introduction

Ceramic fibres are the main component of ceramic matrix composites (CMC's). Several kinds of fibrous reinforcements are used in composites for high temperature applications. Carbon fibres exhibit an excellent mechanical behaviour at high temperatures due to their great microstructural stability under vacuum or inert atmospheres [1]. However they are highly sensitive to oxygen at temperatures as low as 450–500 °C [2, 3]. Oxide fibres, such as alumina or zirconia based fibres [4, 5] are stable under an oxidizing atmosphere, but their density is much higher and their tensile strength and their creep resistance are rather low [6–8]. Silicon carbide fibres appear to be highly attractive candidates for reinforcement in CMC's for high temperature applications. In fact crystalline SiC has both a high stiffness and a good creep resistance in addition to a high oxidation resistance (due to the growth of a protective silica film in the passive oxidation regime) [9–11]. Silicon carbide fibres fabricated by chemical vapour deposition on a tungsten or a carbon core exhibit an excellent tensile strength and a good creep resistance [12] but they are unweavable due to their too large diameter. Furthermore, annealing treatments under an inert atmosphere lead to an unexpected tensile strength loss which is still not well understood [13].

Nanocrystalline SiC-based fibres with a small diameter have been prepared by Yajima and co-workers using a process very similar in its principle to that previously used for the preparation of carbon fibres. This process involves 3 steps: (i) the spinning of an organosilicon precursor (e.g., a polycarbosilane) in the molten state, (ii) an oxygen-curing in order to make the fibres infusible and (iii) the pyrolysis of the filaments leading to the ceramic fibre [14, 15]. Two commercial SiC-based fibres produced using this technique are available; Nicalon fibre (from Nippon Carbon) and Tyranno fibre (from UBE) [16]. Nicalon fibre has been studied by many authors: it mainly contains β-silicon carbide but also free carbon ($\approx$15 at %) and oxygen in a significant amount ($\approx$13 at %) which is introduced during the curing process. Its microstructure consists of nanometric crystals of SiC ($\approx$2 nm) and carbon clusters embedded in an amorphous silicon oxycarbide phase SiO_xC_y [17, 18]. Unfortunately, this kind of fibre has a limited thermal stability. When heated above about 1100–1200 °C, the silicon oxycarbide phase undergoes decomposition with an evolution of gaseous species (CO and SiO) and a growth of the SiC grain size,

which leads to a decrease of both the tensile strength and the Young's modulus [19–25]. The thermal stability of ex-organosilicon fibres can be improved by using an oxygen-free curing process. Recently Okamura *et al.* [26] and Takeda *et al.* [27] have proposed a physical curing process (electron beam (EB) or γ-ray irradiation) under an inert atmosphere which leads to a low oxygen content fibre after pyrolysis.

The aim of the present study was (i) the preparation of a model SiC-based fibre with a low oxygen content based on an anaerobic EB-curing process and (ii) its characterization from a chemical, microstructural and mechanical point of view either in the as-prepared state or after annealing under various atmospheres. The final objective was to highlight the main differences between the EB-cured fibre and commercial Si–C–O fibres.

2. Filament processing

The precursor used in the present study was a commercial polycarbosilane (PCS) of theoretical formula $-(CH_3SiH-CH_2)_n-$ obtained from Mitsui (Paris). The melting temperature of the as-received precursor was too high for easy spinning. The molecular weight distribution of the PCS was adjusted by performing an extraction with a suitable solvent, i.e., ethyl-acetate, which eliminated species with high masses. This was followed by a heat treatment at 300 °C under vacuum, which eliminated any solvent and low molecular mass species.

The precursor was spun, in the molten state under a nitrogen atmosphere, with laboratory apparatus, equipped with a single-spinneret and stretched with a take-up reel, in order to achieve a mean diameter of $\approx 20\,\mu m$ in the solid state. The continuous green monofilament was cut at a length of 400 mm and introduced into a glove-box filled with argon of grade N56 from Alphagaz.

The green filaments were then cured under an electron beam according to the following procedure: (i) they were first placed under the glove-box atmosphere, into flat aluminium containers, that were subsequently tightly sealed, (ii) the containers were then electron beam irradiated (with a rate close to 300 Mrad per h) with a final dose of about 1000 Mrad, (the containers were set in a water-cooled holder in order to avoid the fusion of the filaments) and finally (iii) the irradiated containers were opened in the glove-box in order to avoid any oxygen-contamination before pyrolysis. The electron beam-cured filaments were placed into a silica boat which was transferred to the pyrolysis furnace whose silica tube was connected to the glove-box.

The fibres were then pyrolysed under a flow of high-purity argon ($Q = 1\,l \cdot h^{-1}$, $P = 100\,kPa$), up to 850 °C for 1 h with a relatively slow heating rate ($50\,°C \cdot h^{-1}$) in order to avoid the formation of volume flaws which might result from gas elimination and densification occurring during the organic-mineral transition. After this treatment, the fibres that were no longer sensitive to oxidation, could be handled in air.

The pyrolysis was then achieved with a high-temperature pyrolysis equipment (1800 °C) comprising a graphite crucible heated with a radio frequency coil. The samples were heated ($60\,°C \cdot min^{-1}$) and maintained at the pyrolysis temperature T_p (with $1000 < T_p < 1750\,°C$) under a high-purity argon or nitrogen atmosphere (100 kPa) during a time t_p ($0.25\,h < t_p < 1\,h$).

3. Characterization of the filament

The average molecular weights were determined by gel permeation chromatography (GPC), using five μ-styragel columns (porosity ranges of 10, 50, 10^2, 10^3 and 10^4 nm) and tetra-hydro-furan (THF) as the eluent at a flow rate of $1\,ml\,min^{-1}$. Molecular weights were calibrated with polystyrene standards (eleven points on the calibration curve, the detection system being a Wasters Associates differential refractometer R401).

The thermogravimetric analyses (TGA) (TGS 2 apparatus from Perkin Elmer) were performed, up to 950 °C, in platinum crucibles on 10–50 mg samples under a pure argon flow (flow rate: $1\,l \cdot h^{-1}$) with a temperature increase rate of $5\,°C \cdot min^{-1}$.

The infrared (IR) spectra were recorded in the transmission and the Fourier transform modes (FTIR) in the 400–4000 cm^{-1} range (Perkin Elmer 1420 or 683 spectrometers), from pressed pellets made from a mixture of KBr powder and the finely ground samples (weight ratio: 1%) under an inert atmosphere, for the precursor and the pyrolytic residues.

The gases formed during the pyrolysis of chips of the precursors or the cured-fibres (as described above) were analysed by mass spectrometry. The mass spectrometer (Delsi Nermag Anagaz 200) was connected to the pyrolysis furnace outlet in order to analyse the gases diluted by the argon flow.

Elemental analyses were performed on polished cross-section samples (chips of pyrolytic residues or fibres) according to electron probe microanalysis (EPMA: Camebax 75 from Cameca) in the wavelength dispersion mode (PET (penta-ery tutol) crystal for Si-K_α and a PCII (pseudo crystal multilayer) multilayer for C-K_α and O-K_α) with standards (SiC and SiO_2) whose compositions were assumed to be stoichiometric. The hydrogen content of the samples was not taken into account.

Auger electron spectroscopy (AES) characterization was performed with a scanning microprobe (Phi 5905 AM from Physical Electronics) equipped with an Ar^+ sputtering gun. The variations of the intensities of the Auger electron peaks (Si-LVV; C-KLL and O-KLL) as a function of the sputtering time were used to draw semi-quantitative composition–depth profiles from the sample surface (sputtering rate reference: Ta_2O_5).

The density of the samples was measured by helium-pycnometry (Accupyc 1330, Micromeretics).

The X-ray diffraction (XRD) spectra (Cu-K_α/Siemens D5000 diffractometer) were recorded from tows of fibres for each T_p value. The apparent mean grain size (L) of the β-SiC crystalline phase present in the

samples was calculated from the width (D) of the (111) diffraction peak at mid-height, according to the following equation:

$$L = K\lambda/D\cos\theta \quad (1)$$

where K is a constant (taken as 1), λ the Cu-K_α wavelength (i.e. $\lambda = 0.154$ nm) and θ the Bragg angle ($\theta = 17.8^\circ$ for β-SiC (111)).

The structure of the monofilaments was studied at the nanometer scale by high resolution transmission electron microscopy (TEM) (2000 FX TEM from Jeol). Each sample was glued with silver paint onto a copper grid and ion milled with an Ar^+ sputtering gun (Gatan 600). The TEM analyses were performed in the bright field (BF), dark field (DF) selected area diffraction (SAD) and lattice fringe (LF) image modes to characterize the fibre microstructure.

The electrical conductivity of the fibres was measured using the four-point method, from room temperature to about $-190\,^\circ$C. A single fibre connected to copper wires with silver paint and glued at the end of a thermocouple, was set into a glass vessel under a pure helium atmosphere which was progressively dipped into liquid nitrogen. The data, plotted as a $\mathrm{Ln}\,\sigma = f(1/T)$ graph, σ being the electrical conductivity and $1/T$ the reciprocal temperature, were used to assess the apparent activation energy when the samples exhibited a semi-conducting behaviour.

The morphology changes of the fibres that occurred during the pyrolysis and annealing treatments were studied by scanning electron microscopy (SEM) (Jeol 840 S).

The monofilaments were tensile tested at room temperature with an apparatus similar to that described by Villeneuve *et al.* [28]. For each T_p value, a batch of about 20 monofilaments were tested with a gauge length of $L = 25$ mm and the data were used to determine the mean ultimate tensile stress σ^R and the Young's modulus E. They were also tensile tested at high temperature in air according the following procedure: the fibre specimen was glued at both ends of alumina tubes with an alumina based cement (a hot grips type of assembly with a 25 mm gauge length). It was then mounted onto the same tensile apparatus as that used for the room temperature tests equipped with a furnace that was already at the testing temperature. The high temperature tests were performed within about one minute of the stabilization of the temperature.

The single filaments were submitted to creep tests with cold grips under a pure argon atmosphere at 1300 °C using the creep testing apparatus previously designed and used by Bodet [29] in his study of Nicalon fibres.

The oxidation kinetics of the EB-cured fibres (pyrolysed for 15 min at 1400 °C under pure argon) were studied by thermogravimetric analysis (TGA) (Setaram TAG 24). The experiments were performed on samples of about 50 mg held in a pure alumina crucible and heated up to a maximum temperature T_0 ranging from 1000–1400 °C (heating rate: 60 °C per min. with a 1 h isothermal plateau at T_0) under a flow of pure oxygen ($P = 100$ kPa; $Q = 1\,\mathrm{l}\cdot\mathrm{h}^{-1}$).

4. Results

4.1. Uncured precursor analysis

The softening temperatures (measured on a Kofler hot bench) and mass molecular weights for the as-received and molecular weight-adjusted PCS are listed in Table I. The softening temperature (T_s) range of the as-received PCS is much higher and sharper than that of the treated material. As T_s is raised, an evolution of gaseous species is observed, corresponding to the distillation of low molecular weights species.

Furthermore, the data listed in Table I and the GPC elution curves (Fig. 1) clearly show that the average molecular weight (M_n) is reduced after the treatment (due to the elimination of high molecular weight components) as is the molecular weight dispersion I_p. The rheological properties of the precursor are also changed by the molecular weight adjustment. The observed absorption bands correspond to chemical bonds that have been previously assigned for PCS in organosilicon precursors by other authors [30–33]. Characteristic absorptions for Si–CH_2–Si groups at 1350 and 1040 cm^{-1} were observed in addition to the typical silane functional groups, δ(Si–CH_3) at 1260 cm^{-1}, ρ(CH_3–Si) at 830 cm^{-1} and ν(Si–H) at 2130 cm^{-1}.

The IR-spectra of PCS is shown in Fig. 2a. The main absorption bands that were observed are listed in Table II. Aliphatic groups ν(C–H) were also detected at 2800–3000 cm^{-1}. Si–Si and C–C bands were not observed on the spectra (they would be expected respectively at 400 cm^{-1} (ν(Si–Si)) and at 1450 cm^{-1} (δ(C–H))).

TABLE I Some properties of the as-received and molecular weight adjusted PCS

	As-received PCS	Weight adjusted PCS
Softening temperature (°C)	> 250	220
Average molecular weight (M_n)	1530	1160
Polymolecularity (I_p)	2.74	1.86
Ceramic yield at $T_p = 950\,^\circ$C (%)	67.4	55.9

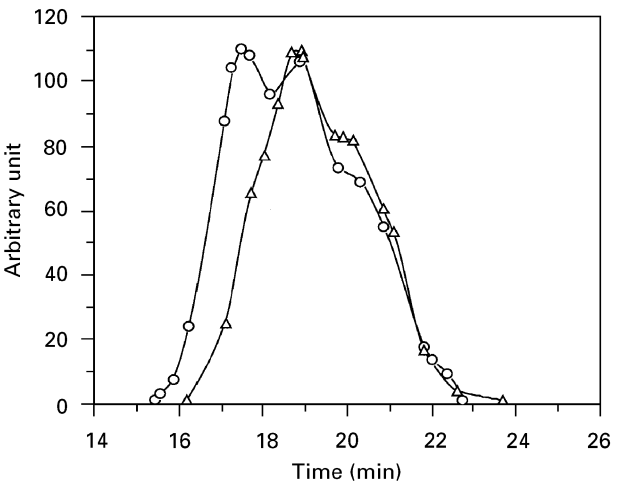

Figure 1 GPC curves for the as-received (○) and molecular weight-adjusted PCS (△).

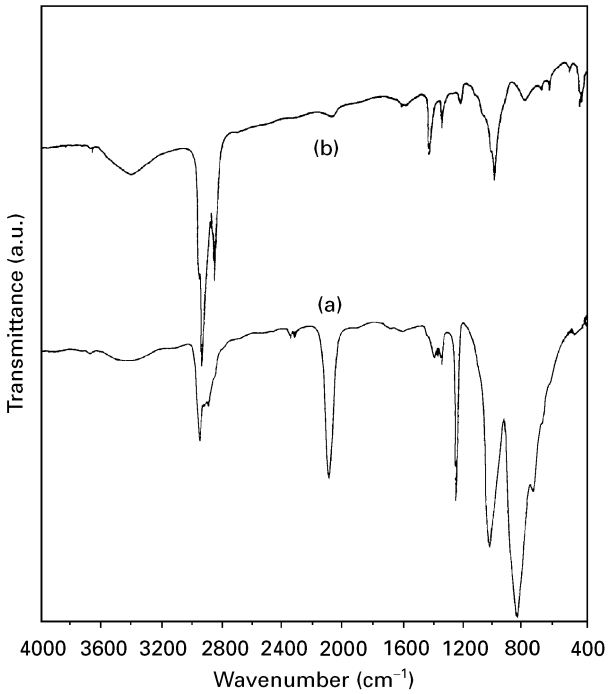

Figure 2 IR spectra of (a) uncured and (b) EB-cured PCS.

On the basis of these data and previously reported data, a model of the polymer was developed.

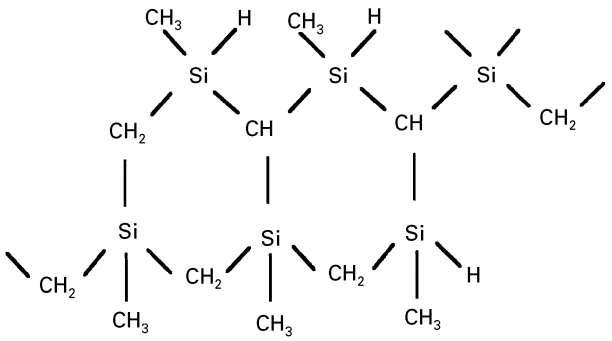

However, the occurrence in the precursor, of silicon atoms bonded to four carbon was also expected, i.e., $(CH_2)_2$–Si–$(CH_3)_2$; $(CH_2)_3$–Si–CH_3 or $(CH_2)_4$–Si, resulting from the thermal cross-linking of the PCS [31, 32, 34].

The variations of the weight loss $\Delta m/m_0$ as a function of temperature during pyrolysis are shown in Fig. 3 for both molecular weight-adjusted PCS and as-received PCS. In both cases, the weight loss during pyrolysis occurred in two main steps. The first one corresponds to the 280–450 °C temperature range. At 450 °C, the weight loss of the treated PCS is higher than that of the untreated one (30% versus 7%). The second step occurs in the 450–700 °C domain in which the weight loss is nearly the same for both of the PCS. The final weight losses at 950 °C under argon for the as received and molecular weight adjusted PCS, are 32.6% and 44.1% respectively.

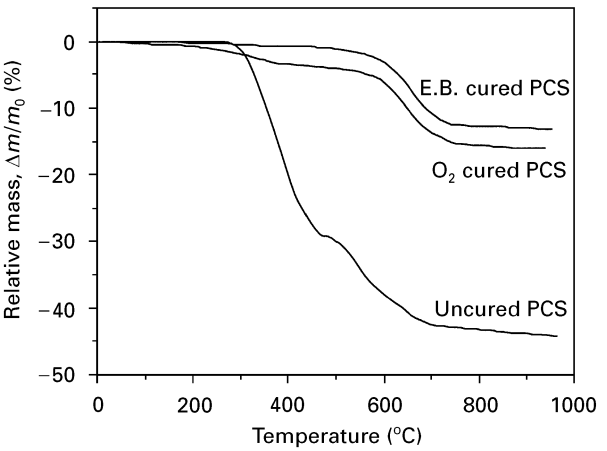

Figure 3 TGA under flowing argon (heating rate = 5°C per min, P = 100 kPa) of as-received and molecular weight-adjusted PCS.

4.2. Electron-beam cured PCS analysis

The irradiated containers were opened under an argon atmosphere in a sealed silica tube, connected to a mass spectrometer which detected the presence of hydrogen resulting from the curing process.

The IR spectra of uncured and cured PCS are shown in Fig. 2(a and b). The absorption bands which characterize the Si–H bond (valence vibration (ν) at 2100 cm^{-1}, deformation vibration (δ) at 850–940 cm^{-1}) and the Si–CH_3 functions (deformation $\delta_a(CH_3)$ at 1410 cm^{-1} and $\delta_s(CH_3)$ at 1250 cm^{-1}) have strongly decreased during the EB-curing (the ν(Si–H) band has almost disappeared). In comparison with the δ(Si–CH_3) band, Si–CH_2–Si characteristic bands (ω(CH_2) at 1020 cm^{-1} and δ(CH_2) at 1350 cm^{-1}) have increased after the curing treatment. Severe modifications of the precursor structure have thus occurred during the EB-curing which result in

TABLE II Main absorption bands observed in the IR spectra of PCS and its pyrolytic residues. vs: very strong; s: strong; m: medium; w: weak

Wavenumber (cm^{-1})	Intensity	Assignment	Wavenumber (cm^{-1})	Intensity	Assignment
2950	m	$\nu_a(CH_3)$	1350	w	δ(CH_2) (Si_2C)
2920	m	$\nu_a(CH_2)$	1250	s	δ_s(Si–CH_3)
2900	m	$\nu_s(CH_3)$	1020	s	ω(CH_2) (Si_2C)
2850	m	$\nu_s(CH_2)$	800–985	s	δ(Si–H)
2100	vs	ν(Si–H)	760–860	s	ρ(CH_3–Si)
1450	m	δ(C–H)	450	w	ν(Si–Si)
1410	w	δ_a(Si–CH_3)			

noticeable changes in the IR-spectrum. These changes include; (i) the $\omega(Si–CH_2–Si)$ band strongly decreases with respect to the $\nu(C–H)$ bands at 3000–2850 cm^{-1} (ii) the C–C characteristic band appears after curing ($\delta(CH_2)$ at 1450 cm^{-1}) and (iii) a weak band at 450 cm^{-1} increases which could be due to the $\nu(Si–Si)$ stretching.

4.3. Pyrolysis of the uncured and EB-cured precursor

4.3.1. FTIR analysis

The IR spectra of the PCS and the pyrolytic residues are shown in Fig. 4 for increasing pyrolysis temperatures, ranging from 600–1200 °C.

4.3.1.1. A pyrolysis temperature of 600 °C. All the absorption bands noted in the previous spectra are still present at 600 °C. This suggests that the precursor retains its organosilicon character at this temperature. However, an evolution in the relative intensities of the absorption bands is observed between room temperature and 600 °C in that (i) the strong absorption bands at 2100 and 1250 cm^{-1}, respectively assigned to $\nu(Si–H)$ and $\delta_s(Si–CH_3)$ have decreased in intensity, (ii) the weak absorption bands at 2950 cm^{-1} and 1410 cm^{-1} respectively assigned to $\delta_a(C–CH_3)$ and $\delta_a(Si–CH_3)$ have decreased with respect to the nearest bands at 2915 and 1355 cm^{-1} which are assigned to $\nu(CH_2)$ in $C–CH_2–C$ and $\delta(CH_2)$ in $Si–CH_2–Si$ and finally, (iii) the ($Si–CH_2–Si$) characteristic bands namely $\delta(CH_2)$ in $Si–CH_2–Si$ at 1355 cm^{-1} and also the strong and wide band $\omega(CH_2)$ in $Si–CH_2–Si$ at 1040 cm^{-1} have increased.

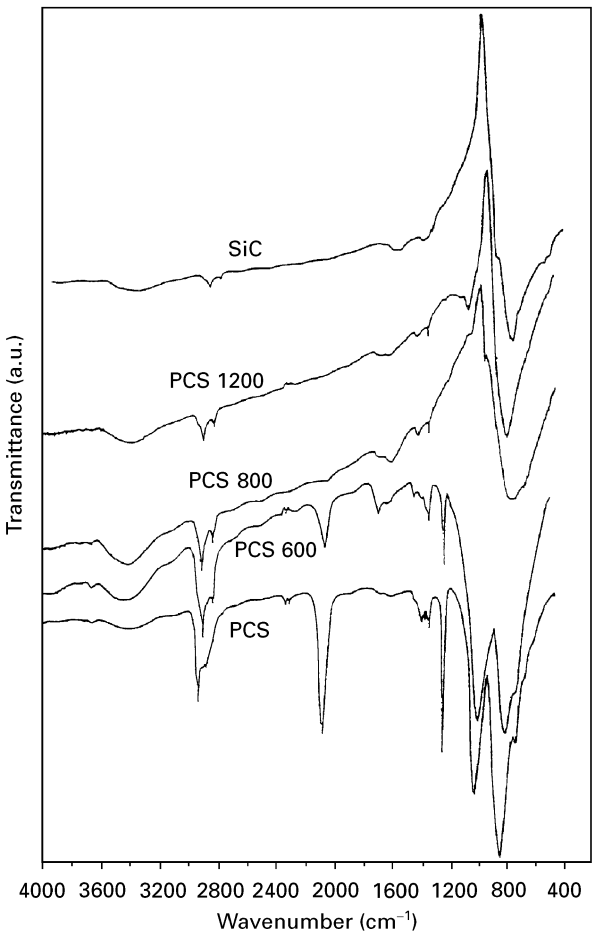

Figure 4 IR-spectra of PCS and its pyrolytic residues at increasing pyrolysis temperatures and of SiC (given as a reference).

4.3.1.2. A pyrolysis temperature of 900 °C. From 600–900 °C, a dramatic decrease of the absorption band intensities is observed for the $\nu(C–H)$ massif at 2850–3000 cm^{-1}, which consists of the $\nu(Si–H)$, the $\delta(CH_2)$ in $Si–CH_2–Si$, the $\delta_s(Si–CH_3)$ and the $\omega(CH_2)$ in $Si–CH_2–Si$. These strong changes are assigned to the organic/mineral transition which occurs within this temperature range. However, the ratio between the intensities of the $\nu(CH_2)$ absorption band at 2915 cm^{-1} and the $\nu_a(CH_3)$ at 2950 cm^{-1} (or $\nu_s(CH_3)$ at 2900 cm^{-1}) has continued to increase as compared to its level at 600 °C.

4.3.1.3. A pyrolysis temperature of 1200 °C. Only minor changes in the absorption spectrum are observed from 900–1200 °C. These changes are (i) the absorption band $\nu(C–H)$ at 2900 cm^{-1} is observed to have a lower intensity. Considering that this is a SiC spectrum, the observed intensity is probably due to a contamination due to the grinding in the mortar rather than the occurrence of residual aliphatic C–H bonds in the material, (ii) the broad absorption band at 815 cm^{-1}, which is assigned to silicon carbide, becomes sharper and similar to that for a pure SiC spectra.

4.3.2. Thermogravimetric analysis

4.3.2.1. PCS fibre analysis. TGA curves of untreated PCS, EB-cured PCS and oxygen-cured PCS are shown in Fig. 5a. The pyrolysis of the uncured PCS seems to involve two steps: (i) a first step, up to 500 °C with a 30% weight loss and (ii) a second step from 500–700 °C with a final ceramic yield of 56%. Conversely, that of the EB-cured PCS seems to occur in a single step from 500–750 °C, leading to a much higher ceramic yield (87%).

An oxygen-cured PCS TGA curve shows that a 4% weight loss takes place at low temperatures (from 200–500 °C) and that the final pyrolysis (in the range 500–900 °C) leads to a similar weight loss to that for the EB-cured PCS (about -13 wt %).

4.3.2.2. Si–C fibre analysis. Both the Si–C fibres, prepared at T_p 1400 °C (with an isothermal plateau of 15 min) under argon and the commercial Si–C–O (Nicalon CG, NL 202) were submitted to the thermogravimetric analyses. The TGA curves are plotted in Fig. 5b. The Si–C–O fibre undergoes a large weight loss within the temperature range $1350 < T < 1700$ °C, with a final value of $\Delta m/m_0 = -26\%$ at $T = 1800$ °C. Conversely, no significant change is observed for the Si–C fibre up to $T = 1600$ °C. Only

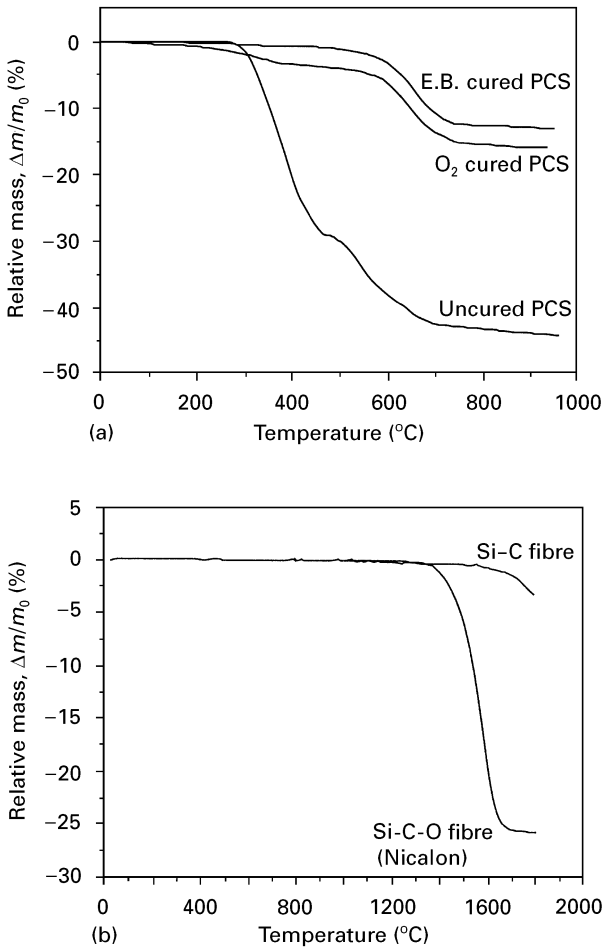

Figure 5(a) TGA curves of uncured, oxygen-cured [36] and E.B.-cured PCS filaments under flowing argon (heating rate = 5 °C per min, $P = 100$ kPa) and (b) TGA under flowing argon (heating rate = 10 °C per min $P = 100$ kPa) of (●) Si–C ($T_p = 1400$ °C, $t_p = 15$ min) and Si–C–O (Nicalon) fibres.

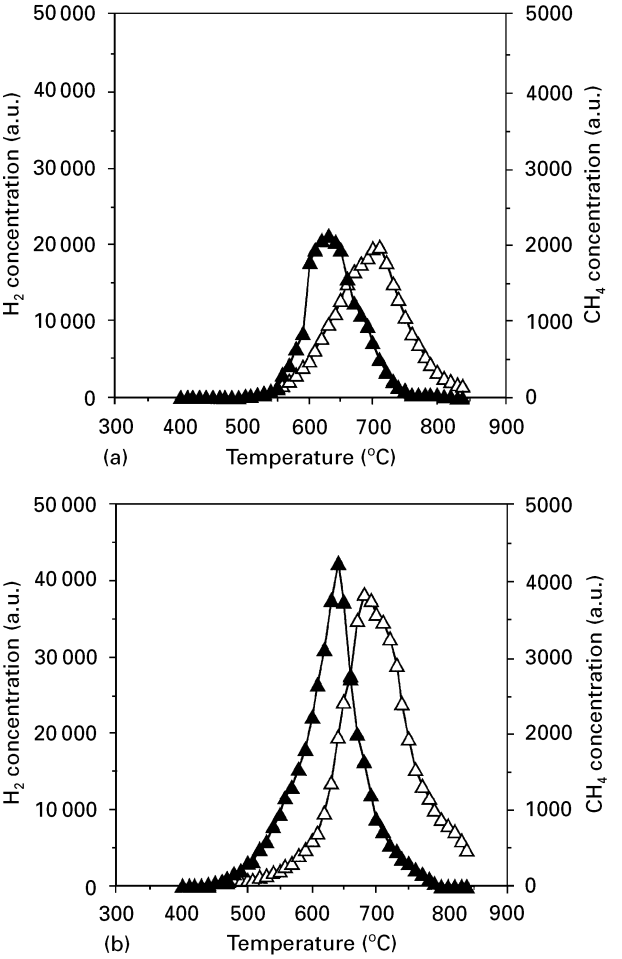

Figure 6 Variations of the (△) hydrogen and (▲) methane concentrations (assessed by mass spectroscopy) in flowing argon ($P = 100$ kPa, $Q = 1$ l per h) as a function of temperature (ramp: 50 °C per h) during the organic/inorganic transition of uncured (a) and E.B.-cured (b) PCS filaments.

a slight and progressive weight loss is recorded beyond $T = 1600$ °C, with $\Delta m/m_0 = -3\%$ at $T = 1800$ °C.

4.3.3. Gas analysis

Gas analyses were performed during the pyrolysis of as spun PCS filaments and EB cured filaments. Hydrogen and methane were analysed as a function of T_p, by measuring the intensities of mass spectra peaks corresponding respectively to the molecular masses 2 and 15 (Fig. 6).

The gas evolution from uncured and cured PCS filaments are very similar, except for the intensities, suggesting that the gas evolution (both hydrogen and methane) for the cured filaments is apparently more important than that for the uncured filaments. For the uncured PCS, low molecular weight species might condense on to the cold parts of the pyrolysis furnace, while no low-volatility products were observed during the pyrolysis of the EB-cured filaments. The evolution of methane is observed from 450–500 °C with a maximum at 630–650 °C, whilst hydrogen is detected at a higher temperature (500–550 °C) with a maximum at 700 °C. At 850 °C, the formation of hydrogen is still detected but it decreases continuously when the temperature is maintained at 850 °C, while no significant methane emission is detected beyond 800 °C.

4.3.4. Elemental analysis of the pyrolysed precursor and the ceramic fibres

4.3.4.1. Bulk analysis. EPMA were performed on (i) the residues from uncured PCS filament pyrolysis and (ii) on ceramic fibres after the EB curing and pyrolysis (Tables III and IV). It is noteworthy that this technique does not take into account any hydrogen in the ceramic (which might be present in significant quantities below 1400 °C [34, 35]).

It clearly apparent that no significant changes in the chemical composition is observed in the pyrolytic residues due to (i) the molecular weight adjustment of the as-received PCS, (ii) the spinning process and (iii) the EB-curing treatment of the PCS filaments.

After pyrolysis, one batch of EB-cured fibres was observed to exhibit a much higher oxygen content (≈9 at %), which is probably due to one of the containers that had been used in the EB-curing not being tightly sealed. As a consequence, the EB exposure was not performed under an inert atmosphere but instead under an oxidative O_2/H_2O environment. This batch was not further investigated in the present study except for mechanical tests in order to assess the influence of the oxygen concentration on the thermal stability and the mechanical behaviour of the fibres. Three fibres with different oxygen concentrations were

TABLE III Elemental composition of the PCS pyrolytic residues at 900 °C, as derived from EPMA (hydrogen is not taken into account)

Materials	As-received PCS	Weight-adjusted PCS	As-spun PCS filaments	EB-cured PCS filaments
Silicon (at %)	39	39	38	39.5
Carbon (at %)	59	59	59.9	57.5
Oxygen (at %)	2	2	2.5	3
C/Si (at %)	1.51	1.51	1.58	1.46

TABLE IV Elemental composition of the EB-cured ex-PCS fibres pyrolysed at increasing temperature T_p as derived from EPMA (hydrogen is not taken into account)

T_p (°C)	900/ Ar	1000/ Ar	1200/ Ar	1400/ Ar	1600/ Ar	1600/ N_2
Silicon (at %)	39.5	40	40	39	40	39
Carbon (at %)	57.5	57	57	58	57	58
Oxygen (at %)	3	3	3	3	3	3

investigated, $C_{(O)} = 3$ at % (EB-cured), $C_{(O)} = 9$ at % (O_2/EB-cured) and $C_{(O)} = 19$ at % (O_2-cured [38]), used as the reference material.

The low and constant oxygen concentration produced in the filaments during their preparation shows that, as expected, all the processing steps were performed under low oxygen concentration conditions. No change in the chemical composition in the bulk of the fibres was observed up to heat treatments of 1600 °C, for 1 h, under an argon or nitrogen atmosphere.

4.3.4.2. Chemical analysis of the fibre surface. The AES analysis shows that a thin carbon layer appears for $T_p \geqslant 1400$ °C and continues to grow as T_p and/or t_p are raised. As an example, the thickness of the carbon layer is about 50 nm for $T_p = 1600$ °C and $t_p = 15$ min, irrespective of whether the fibres are pyrolysed under argon or nitrogen (Fig. 7a and b). The chemical composition below this carbon layer is observed to be the same as that of the core of the fibre, as determined by EPMA.

After heat treatment at 1600 °C under a nitrogen atmosphere, a small amount of nitrogen is also observed in a 100 nm thick zone (Fig. 7b) at the surface of the fibre.

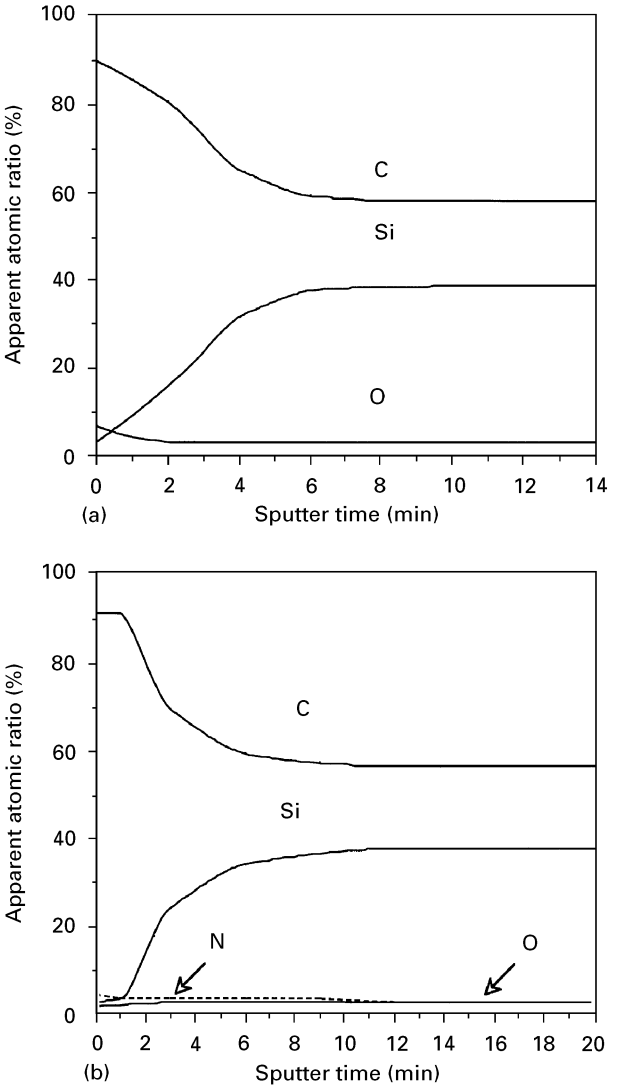

Figure 7 AES depth concentration profiles for Si–C fibres treated at $T_p = 1600$ °C (a) under argon (b) under nitrogen. The sputtering rate was 10 nm per min and Ta_2O_5 was used as a reference.

4.3.5. Structure and microstructure of the EB cured fibres

4.3.5.1. XRD analysis. For $T_p < 1200$ °C, the fibre microstructure is observed to be amorphous, since no diffraction peaks are detected. For $T_p \geqslant 1200$ °C, three main peaks, assigned to the (111), (220) and (311) reflections of β-SiC are observed (corresponding respectively to a d spacing of 0.251, 0.154 and 0.131 nm) (Fig. 8).

From $T_p = 1200$–1750 °C, the material undergoes crystallization. A slight increase, in the grain size (calculated from the width of the (111) reflection) is observed from 1200–1600 °C, with a mean value of about 4 nm at 1200 °C and 6 nm at 1600 °C (Fig. 9). Beyond this temperature, the grain size increases more rapidly (about 10 nm at 1750 °C for $t_p = 1$ h) but remains considerably lower than for Si–C–O fibres [36, 37].

4.3.5.2. TEM analysis. These analyses were performed on ion-milled fibres using the dark field, lattice fringe

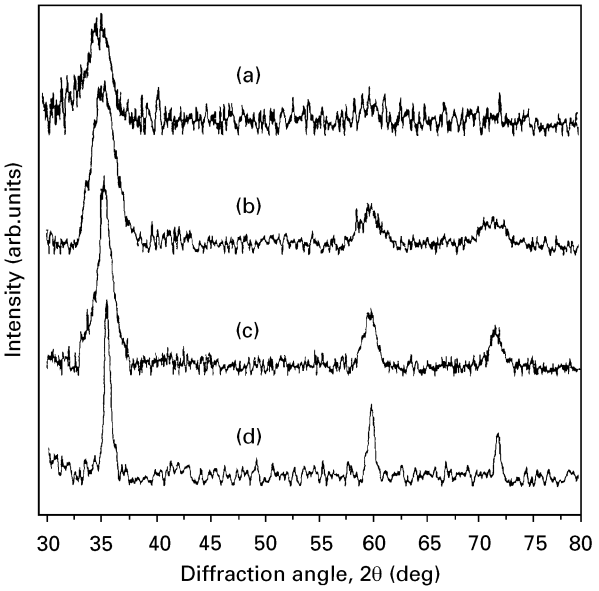

Figure 8 XRD spectra of heat-treated fibres under pure argon (100 kPa). (a) $T_p = 1200\,^{\circ}C$, $t_p = 15$ min; (b) $T_p = 1400\,^{\circ}C$, $t_p = 15$ min; (c) $T_p = 1600\,^{\circ}C$, $t_p = 15$ min and (d) $T_p = 1750\,^{\circ}C$, $t_p = 1$ h.

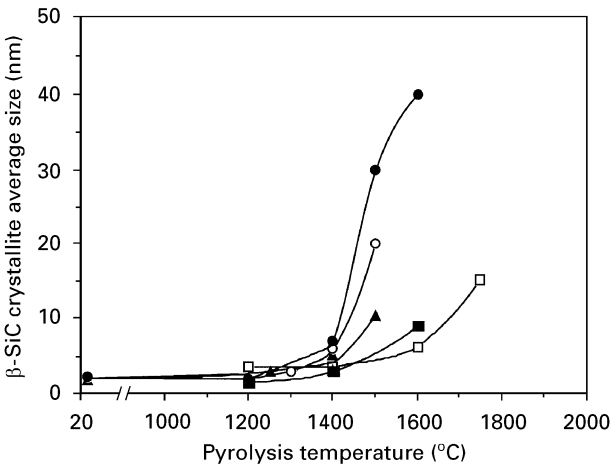

Figure 9 β-SiC crystallites average size as a function of pyrolysis temperature T_p for Si–C–O (Nicalon) fibre assessed from (○) XRD analysis [36] (●) TEM analysis [36], (▲) TEM analysis [37]. Data is presented for the Si–C fibre that has been measured in the present work using (□) XRD analysis and (■) TEM analysis. The pyrolysis durations were all 15 min with the exception of the XRD data taken on the Si–C fibre where the duration was 1 h.

and SAD modes in order to characterize the organization of both the SiC and the free carbon phases present in the fibre.

For $T_p = 1200\,^{\circ}C$, the fibre consists of very small β-SiC crystallites: i.e., 2–3 nm, a result in agreement with the XRD analysis (Fig. 10a). LF imaging also shows free carbon in the bulk, as isolated basic structural units (BSU) (i.e., 2 or 3 aromatic layers of about 10 aromatic carbon cycles) visible in Fig. 11a.

When treated at 1400 °C, the fibre is polycrystalline with; (i) a mean SiC apparent grain size of about 4 nm (Figs 10b and 11b), and (ii) an intergranular phase, consisting of turbostratic carbon layers. This carbon is rather well organized into turbostratic stacks of 3–5 carbon layers, partly surrounding SiC crystals

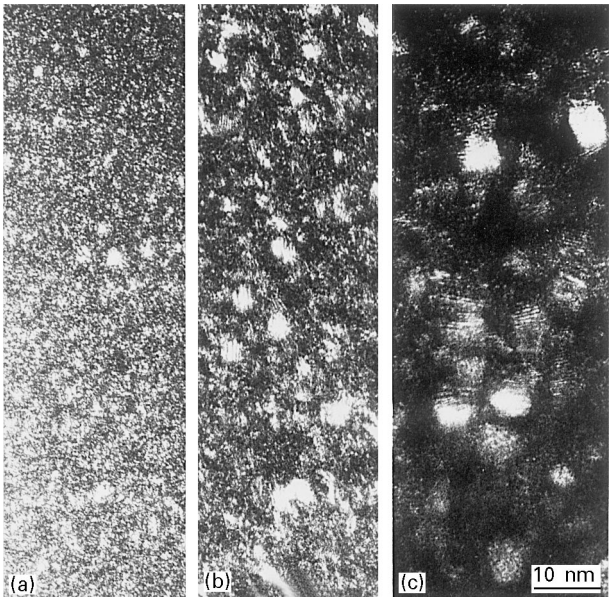

Figure 10 111-SiC dark field TEM micrographs of the fibre annealed 15 min under argon (a) $T_p = 1200\,^{\circ}C$, (b) $T_p = 1400\,^{\circ}C$ and (c) $T_p = 1600\,^{\circ}C$.

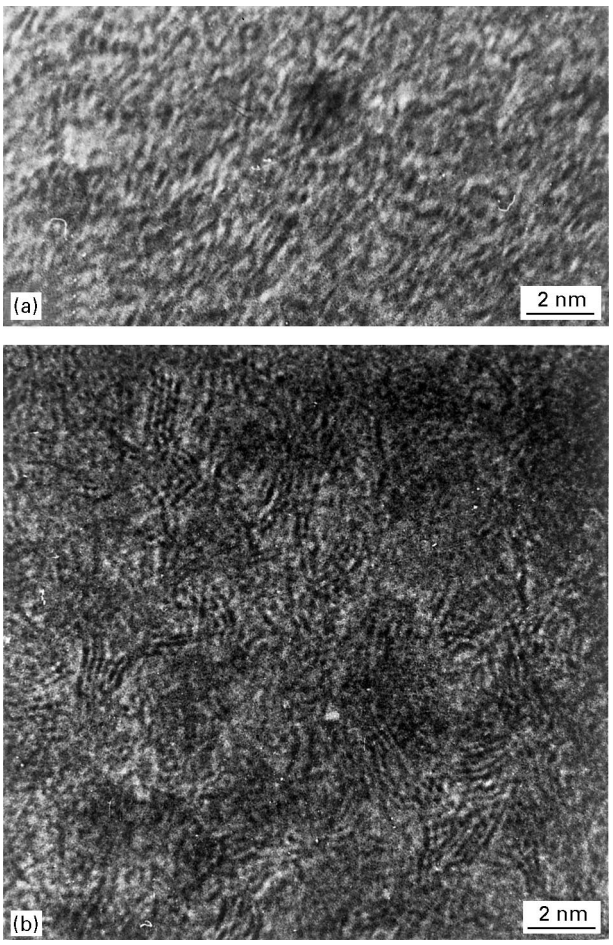

Figure 11 HRTEM micrograph of the fibre annealed for 15 min under argon at $T_p = 1200\,^{\circ}C$ (a) and at a $T_p = 1400\,^{\circ}C$ (b).

(Fig. 11b). The SiC and carbon crystallites do not exhibit any preferential orientation.

The SiC grains continue to grow between 1400–1600 °C. The crystallite size is of the order of 8–10 nm as determined locally by DF analysis (Fig. 10c).

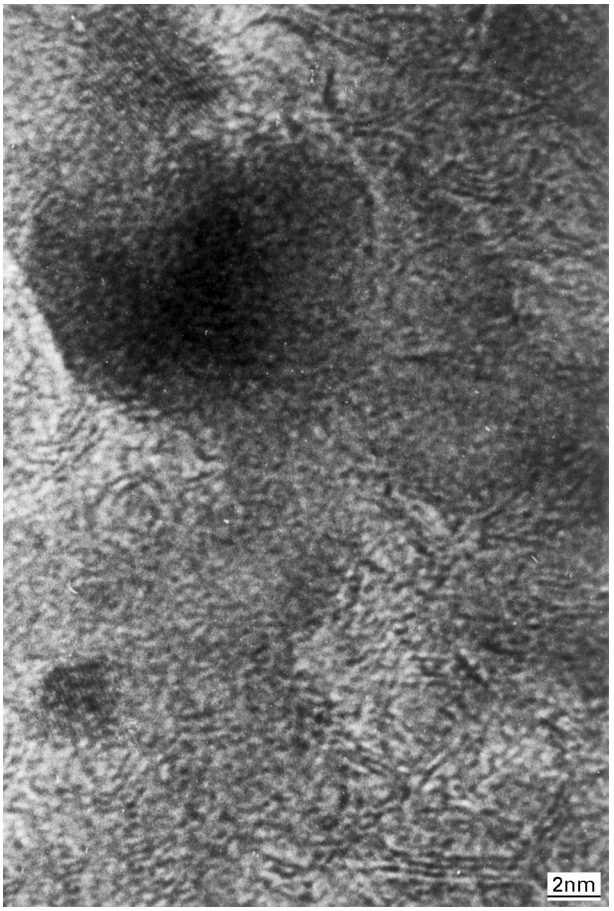

Figure 12 HRTEM micrograph of the fibre annealed for 15 min under argon at $T_p = 1600\,^{\circ}C$.

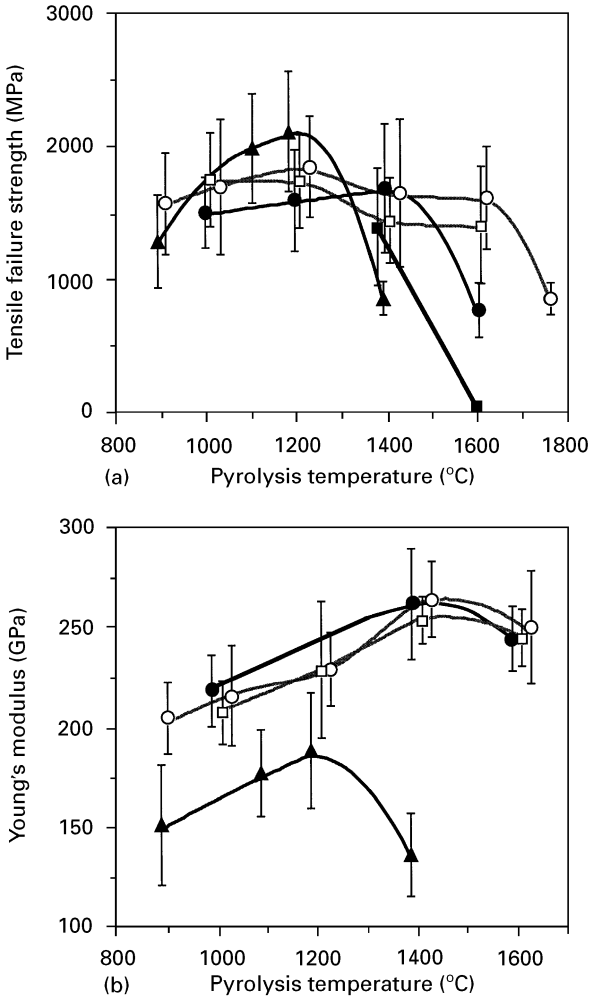

Figure 13 Variations of the tensile failure strength and Young's modulus at ambient of oxygen-cured (O = 19 at %), oxygen/EB-cured (O = 9 at %) and E.B.-cured fibres (O = 3 at %) pyrolysed at increasing temperatures T_p under an argon or nitrogen atmosphere (100 kPa) (▲) O_2-cured under argon [38], (■) O_2/EB-cured under argon, (–□–) O_2/EB-cured under nitrogen (–●–) EB-cured under argon and (–○–) EB-cured under nitrogen).

However, the kinetics of growth of SiC are much lower than those reported for oxygen-cured fibres at 1600 °C (i.e., the SiC grain size at this temperature is $\approx$200 nm). Additionally, some reorganization of the intergranular carbon is observed: in particular; (i) the extent of the turbostratic layers is larger (a few tens of nm), (ii) a polygonal shell ordering is still visible (arrowed in Fig. 12) with a larger size, and (iii) an additional poorly organized carbon is observed.

4.4. Mechanical characteristics of the fibres

4.4.1. Mechanical behaviour at room temperature

The variations of the tensile failure strength and Young's modulus measured at room temperature of the fibres as a function of the pyrolysis temperature (for $t_p = 15$ min) are shown in Fig. 13.

4.4.1.1. Fibres pyrolysed under argon. The tensile strength (σ^R) increases as T_p is raised from 1000 to 1400 °C with a maximum close to 1700 MPa for the EB-cured fibres, and 1400 MPa for the O_2/EB-cured fibres. A significant decrease is observed for $T_p = 1600\,^{\circ}C$ with $\sigma^R = 800$ MPa for the EB-cured fibre and almost 0 MPa for the EB/O_2-cured fibre. As a comparison, the tensile strength of the oxygen cured fibres [38] increases with an increasing pyrolysis temperature up to 1200 °C and decreases beyond this value.

4.4.1.2. Fibres pyrolysed under nitrogen. The tensile strength of the EB-cured fibres pyrolysed under nitrogen does not decrease significantly until a pyrolysis temperature of 1600 °C (for $t_p = 15$ min) with σ^R being close to 1800 MPa for the EB-cured fibres and 1400 MPa for the EB/O_2-cured fibres. However, a significant drop occurs beyond this value.

Generally speaking, the Young's modulus (E) increases regularly up to 1400 °C ($E \approx 250$ GPa for both the EB and EB/O_2 cured fibres). As a comparison, the Young's modulus of the O_2-cured fibre is lower (180 GPa at 1200 °C) and decreases significantly when the temperature is further increased to 1400 °C.

Examples of failure surface SEM micrographs are shown in Fig. 14(a and b). At 1600 °C, the failure surface of the fibres is that of a vitreous material whereas the fibre pyrolysed at 1750 °C is clearly crystallized.

4.4.2. High temperature tests in air

The high temperature mechanical tests performed in air, on an EB-cured fibre that had been previously

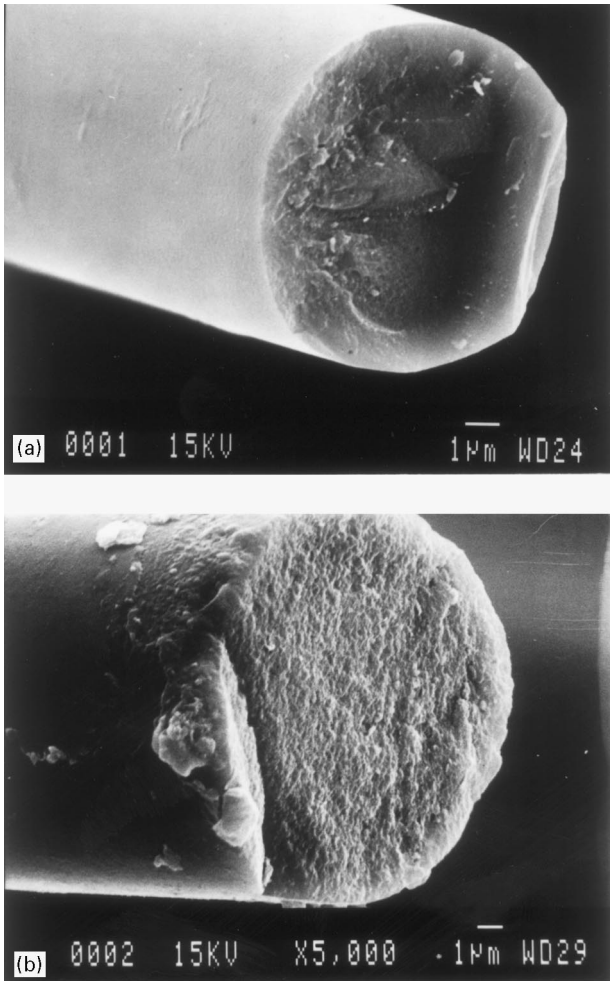

Figure 14 SEM micrographs of the failure surface of annealed fibres under pure nitrogen (100 kPa) for (a) $T_p = 1600\,^{\circ}C$ and $t_p = 15$ min (a) and for (b) $T_p = 1750\,^{\circ}C$ and $t_p = 1$ h.

treated at 1600 °C under nitrogen, show that the tensile strength remains constant from ambient to 1400 °C whereas that for the standard Nicalon fibres regularly decreases within the same temperature range (Fig. 15). However, at 1200 °C the strength is similar for both materials.

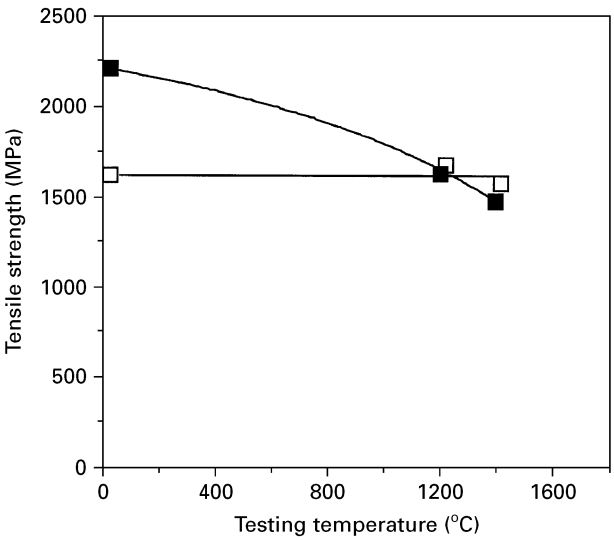

Figure 15 Tensile failure strength as a function of testing temperature in air.

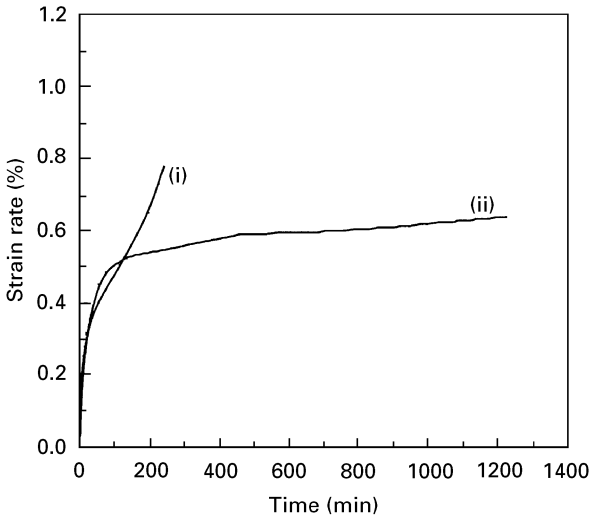

Figure 16 Creep curves for (i) Si–C–O Nicalon and (ii) EB-cured fibres tested in argon. Data taken on samples for which $T = 1300\,^{\circ}C$ and $T = 0.45$ GPa.

4.4.3. Creep tests at high temperature in argon

Creep tests have been performed on both the EB-cured single filaments (pyrolysed at 1400 °C for 15 min under nitrogen) and the Si–C–O fibres (Nicalon NL 202) at 1300 °C under pure argon (100 kPa) (under conditions of stability of the EB-cured fibre) with an applied load of 0.45 GPa. The creep curves show a short domain of primary creep and a rather long steady-state creep domain for the EB-cured fibres (Fig. 16). However, no secondary-state creep domain is observed for the Si–C–O fibre (owing to the short life time and the thermal instability of the fibre at this temperature). The creep rate of the Si–C–O fibre, which has been measured before failure, is much higher than the steady-state creep rate of the oxygen-free fibre ($3.05 \times 10^{-5}\ s^{-1}$ versus $1.22 \times 10^{-6}\ s^{-1}$). On the other hand, the time to failure is significantly lower (250 min. versus 1200 min.).

4.5. Electrical conductivity of the pyrolysed fibres

Electrical conductivity measurements were performed as a function of temperature (from room temperature to − 190 °C) on EB-cured PCS filaments that had been subjected to increasing pyrolysis temperature, (Fig. 17).

At a given test temperature, the electrical conductivity (σ) dramatically increases when T_p is raised from 1000 to 1200 °C (e.g., by four orders of magnitude at 300 K) and more slowly for $1200 \leqslant T_p \leqslant 1600\,^{\circ}C$. These features suggest a transition in the conduction mechanism as the temperature is raised, which seems in turn to be strongly dependent on the microstructure of the fibre.

For pyrolysis temperatures of 1000 and 1100 °C, the fibre exhibits a low electrical conductivity with a typical semi-conducting behaviour (i.e., σ significantly increases as the measuring temperature is raised), with an apparent activation energy, E_a, respectively equal

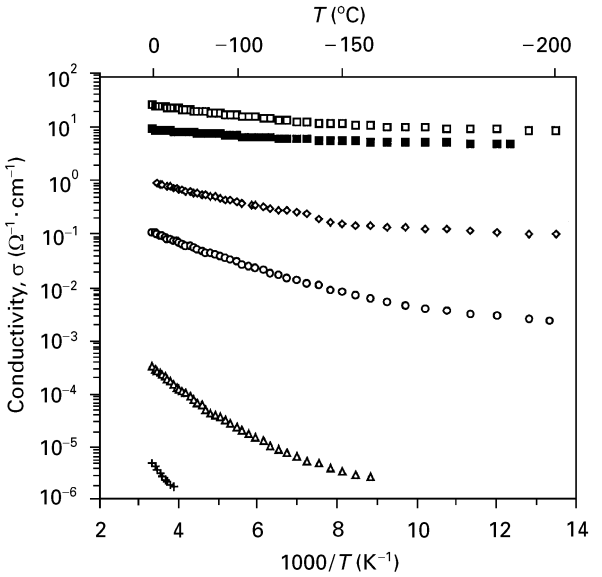

Figure 17 Effect of T_p ($t_p = 15$ min) on the electrical conductivity of Si–C fibres as a function of reciprocal temperature. The T_p values investigated are; (+) 1000 °C, (△) 1100 °C, (○) 1200 °C, (◇) 1400 °C, (□) 1600 °C and (■) 1600 °C with a treatment in air at 600 °C after the pyrolysis.

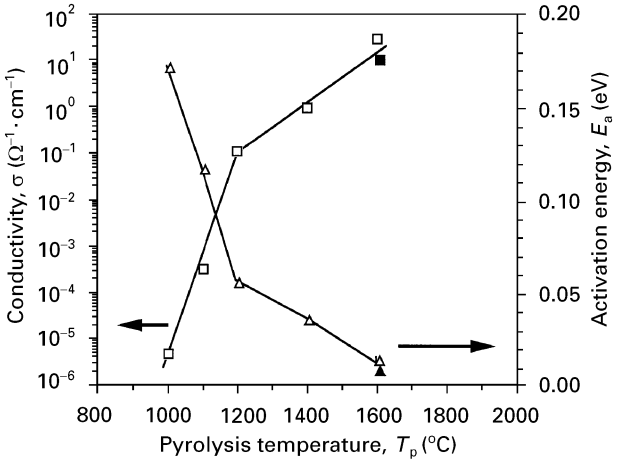

Figure 18 Electrical conductivity (measured at room temperature) (□) and activation energy (determined in the range 200–300 K) (△), as a function of the pyrolysis temperature ($t_p = 15$ min), (▲) and (■) after a treatment in air at 600 °C after pyrolysis.

to 0.172 and 0.117 eV within the temperature range 200–300 K (Fig. 18).

For pyrolysis temperatures between 1100– 1200 °C, σ undergoes a large increase and its temperature dependence is less significant, the activation energy being only 0.056 eV. Finally, for pyrolysis temperatures $\geqslant$ 1400 °C at the electrical conductivity becomes almost independent of the test temperature, as has already been reported for PCS residues when pyrolysed at high temperatures [39], or for heat-treated coals [40].

In order to study the influence of the thin carbon layer formed at 1600 °C on the surface of the fibre on the electrical conductivity, the carbon enriched layer has been removed by a brief oxidation treatment in air at 600 °C. The conductivity of the oxidized fibre is lower than that of the as-pyrolysed fibre but the temperature dependence is almost the same, with a slightly lower activation energy.

4.6. Oxidation behaviour of the EB-cured fibres

4.6.1. Oxidation kinetics

The oxidation kinetics of the filaments were studied by thermogravimetric analysis (TGA) under dry oxygen (10^5 Pa) in the range 1000–1400 °C.

A weight increase is observed whatever the test temperature, the oxidation rate increasing as the temperature is raised. The weight increase is the result of two reactions; (i) the oxidation of SiC into silica, leading to a weight increase and (ii) the oxidation of the free carbon of the fibre, leading to a weight loss (Fig. 19).

The thickness of the silica layer can be inferred from the weight variations, if the specific surface area, the density and the chemical composition of the fibres are known and that the oxide (assumed to be pure silica) is assumed to be homogeneous and its thickness much smaller than the fibre diameter. The oxide sheat morphology and thickness have been studied by SEM and the bulk and surface composition of the fibres determined by EPMA and AES. Density measurements were made by helium pycnometry and the specific surface area was calculated from the fibre diameter measurements.

The silica layer thickness e can be calculated from the value of $\Delta m/m_0$ according to the following equation:

$$\frac{e}{r_0} = K \cdot \Delta m/m_0 \tag{2}$$

where K is a conversion factor and r_0 the initial radius of the fibre. K is defined by the following expression:

$$K = \frac{1}{2} \cdot \frac{M_{SiO_2} \cdot C_{Si}}{M_{SiO_2} \cdot C_{Si} - M_{Si}} \cdot \frac{d}{d_{SiO_2}} \tag{3}$$

where d_{SiO_2} and M_{SiO_2} are the density and the molar mass of silica, M_{Si} is the molar mass of silicon, d and C_{Si} are the density and the silicon mass concentration of the starting fibre. The data for the EB fibres are shown in Tables V and VI.

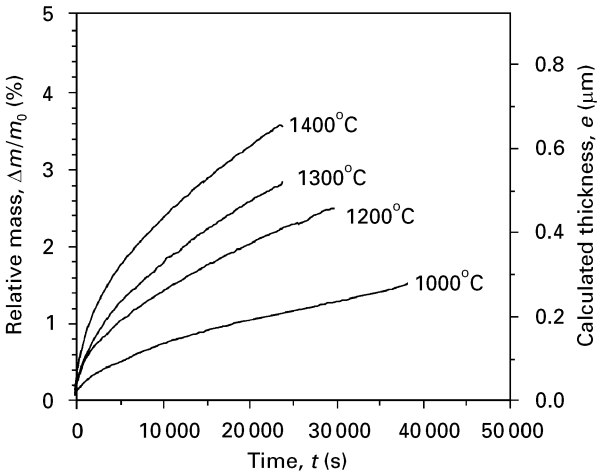

Figure 19 Variations of the relative mass and calculated silica thickness versus time during oxidation under flowing dry oxygen between 1000 °C and 1400 °C ($P = 100$ kPa).

TABLE V Fibre data used in the silica thickness calculations

r_0 (μm)	6
d (g·cm^{-3})	2.73
C_{Si} (wt %)	0.59
K	0.030

TABLE VI Parabolic constant values (k_T) for various oxidation testing temperatures

T(°C)	1000	1200	1300	1400
k_T(μm^2·s^{-1})	1.96×10^{-6}	6.91×10^{-6}	1.11×10^{-5}	1.74×10^{-5}

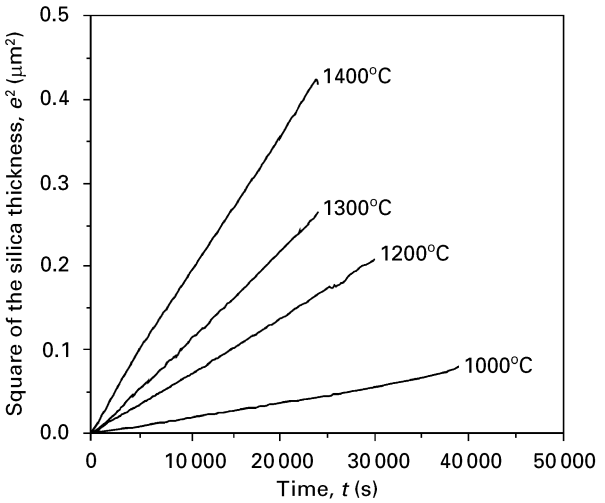

Figure 20 Variations of the square of silica thickness versus time between 1000 °C and 1400 °C during oxidation under flowing dry oxygen ($P = 100$ kPa).

The variations of e^2 as a function of time, obey a linear law (Fig. 20), a feature suggesting that the oxidation kinetics are diffusion-controlled, as has already been observed for silicon and silicon carbide materials [41–44] in addition to Si–C–O and Si–C–N–O fibres [45–47]. The variations of the silica thickness as a function of time can be expressed by:

$$e^2 = e_0^2 + k_T \cdot t \quad (4)$$

where e_0 is the initial thickness of the oxide and k_T is the kinetic constant (Table VI).

The values of k_T, plotted in a Arrhenius diagram (Fig. 21) are observed to obey a linear law:

$$\ln k_T = \ln k_{0T} - \frac{E_a}{RT} \quad (5)$$

where k_{0T} is the pre-exponential constant, E_a the apparent activation energy and R the gas constant.

4.6.2. Morphology of the oxidized filaments

An SEM micrograph of the failure surface of oxidized fibres are shown in Fig. 22. The filaments are coated with a smooth and continuous oxide sheat whose thickness is constant along the fibre periphery. The thickness of the oxide sheat, has been measured for $T_0 = 1000$ and 1400 °C from SEM micrographs, and are reported in Table VII. These values correlate closely with those calculated from the TGA experiments.

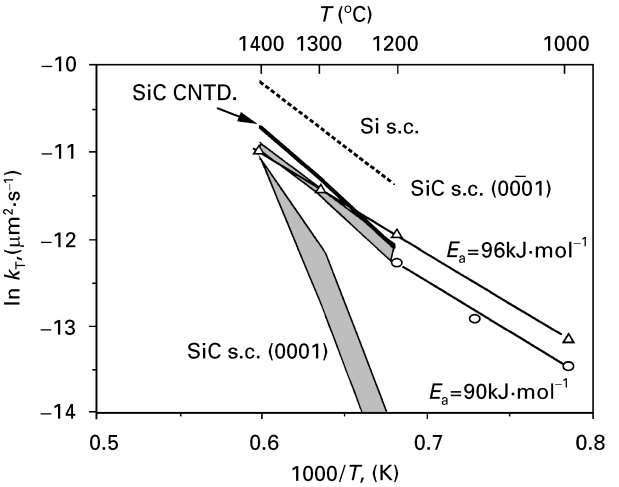

Figure 21 Thermal variations of the oxidation parabolic rate constants for different SiC-based materials: (○) oxygen-cured fibres [44], (△) EB-cured fibres (present work), (- - -) silicon single crystal, (▨) SiC single crystal, (—) polycrystalline SiC crystal (CNTD) [11].

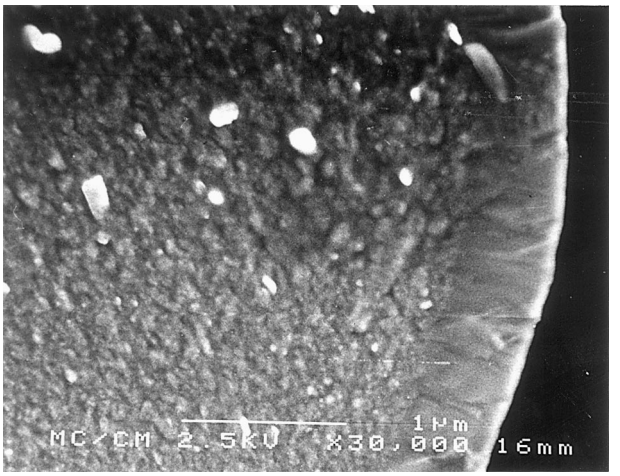

Figure 22 SEM micrograph of the failure surface of an oxidized fibre (7 h at 1400 °C) in pure oxygen (100 kPa).

TABLE VII Comparison of the calculated and measured silica thickness values

Oxidation treatment	11 h (1000 °C)	7 h (1400 °C)
Calculated silica layer thickness (μm)	0.29	0.65
Measured (SEM) silica layer thickness (μm)	0.25	0.63

5. Discussion

5.1. Preparation of the green fibres

Despite its high ceramic yield (67.4%) the as-received PCS precursor has two drawbacks: These are (i) its relativity high oxygen content ($\approx$2 at % after pyrolysis

at 950 °C) and (ii) it is unsuitable for the spinning process due to its high softening temperature. The oxygen contained in the polymer in the form of siloxane functions cannot be eliminated at temperatures less than 1200 °C and is fully converted into a siliconoxycarbide due to the strength of the Si–O bond. Whatever the processing conditions used, the oxygen content of the present PCS -based fibres could not be lowered below 2 at % (for $T \leqslant 1200$ °C) and thus, the priority in the processing of the filaments was to avoid any additional oxygen contamination.

The high molecular weight species are responsible for the high viscosity and the high softening temperature of the as-received polymer (270–280 °C). The lowest mass species induce a gas evolution as the spinning temperature of the precursor is raised (300–310 °C). The molecular weight adjustment removes the highest 50 wt %) and the lowest (only a few wt %) molecular weight species. The average molecular weight and the weight dispersion are thus both reduced. Nevertheless, the elimination of the highest mass species results in a decrease of the ceramic yield (55.3% versus 67.4% for the untreated PCS, at 950 °C).

The oxygen content in the pyrolytic residues is not significantly changed after the molecular adjustment and the C:Si ratio is still equal to 1.51. The viscosity and the softening temperature of the treated precursor are both reduced and green filaments with very small and regular diameter have been spun at 285 °C (ceramic fibres with diameter as low as 10 μm have been obtained). Finally, additional oxygen was not introduced in noticeable amounts during the spinning process.

5.2. Curing of the green fibres

As expected, the 1000 Mrad irradiation treatment is an efficient curing method, since melting of the filament does not occur during the subsequent organic-ceramic transformation. Furthermore, the ceramic yield (after pyrolysis at 950 °C) is significantly increased after irradiation (84% versus 55.3% for the uncured PCS). These features are consistent with the occurrence of a cross-linking of the polymeric structure into a three-dimensional framework. The cross-linking of PCS by EB irradiation has been previously studied by Okamura *et al.* [26] and Takeda *et al.* [27]. It has been shown that the irradiation of PCS results in the formation of free radicals, hydrogen and methane. In the present work, hydrogen was also observed to be formed during the irradiation. It is generally agreed that the bonding between free radicals, during the free radical decaying, results in the cross-linking of the precursor polymer chains and the formation of gas species. Furthermore, it has been found that the free- radical concentration decreases when the treated fibres are annealed at 120–240 °C [26].

The detailed mechanism of the curing process is still not fully understood due to the complexity of the PCS structure. On the basis of the IR spectra of the uncured and cured PCS, the curing mechanism can be described as follows. First, the breaking of Si–H and C–H bonds leading to the formation of free radicals such as:

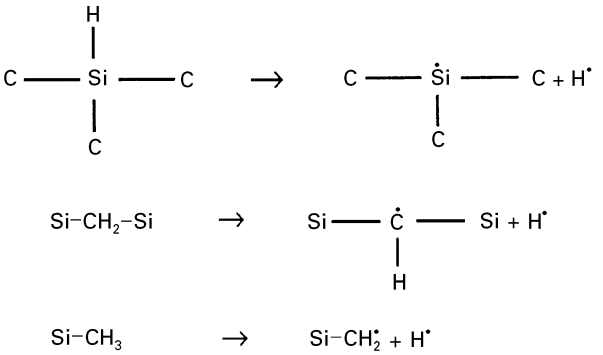

as well as possibly the breaking of the Si–C bonds such as:

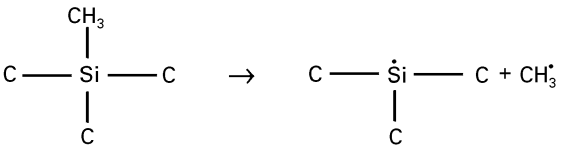

corresponding to the decrease of the Si–CH_3 and Si–H absorption bands. The combination of the free radicals leads mainly to the formation of Si–CH_2–Si bonds (as shown by the relative increase of the 1020 cm^{-1} band due to CH_2 wagging of Si–CH_2–Si) and gas species such as hydrogen (detected in the present work) and to a lesser extent methane [26]. Bonding between free radicals might also create unusual bonds in the PCS, such as Si–Si or C–C since two bands appear after curing which could be assigned to the $\delta(CH_2)$ (at 1450 cm^{-1}) and ν(Si–Si) (at 450 cm^{-1}) vibrations.

The cured filaments, appear to be sensitive to oxidation, as previously noted by Okamura *et al.* [26, 48]. The Si–O–Si absorption band (at 3500 cm^{-1}) is observed to be stronger for the cured fibres than for the uncured fibres. It has been shown that a small amount of free radicals is still present in the bulk of the fibre after irradiation at room temperature [26]. Thus, the increase of the Si–O–Si band might be related to the oxidation of radicals not involved in cross-linking. The oxygen is thought to have been introduced during the preparation of the samples for the FTIR analysis (since the oxygen content of the pyrolysis residues is not significantly increased in the case of the cured filaments).

It should be noted that the IR absorption spectrum of the irradiated PCS fibres is somewhat different from those of similar materials reported by other authors [27, 48]. In the present work, the intensity of the absorption band relative to the wagging of CH_2 in Si–CH_2–Si is significantly reduced after irradiation as compared to that of the C–H stretching for the aliphatic groups (2800–3000 cm^{-1}). Thus, the polymeric framework itself might be affected by the irradiation process. The irradiation dose may have locally exceeded 1000 Mrad, however, the properties

of the cured fibres are not altered (the ceramic yield at 950 °C is rather high (84%) and no fusion of the filaments was observed).

5.3. The organic–inorganic conversion

On the basis of the results reported in section 4, the organometallic–mineral transformation of both the uncured and cured PCS filament can be discussed as follows:

5.3.1. For $300 < T_p < 450$ °C

The first important weight loss (i.e., 30 wt %) at $300 < T_p < 400$ °C is observed for the green filaments (and) is assigned to the evolution of oligomers condensed in the cold parts of the pyrolysis apparatus. No light gaseous species are detected in the gas phase, indicating that no chemical reactions occur within that temperature range. For the cured filaments, no significant weight loss is observed up to 500 °C which is contrary to what has been reported for the oxygen-cured fibres [39] (4% wt loss). This very low weight loss (almost nil for EB-cured fibres) with respect to that of the uncured PCS, indicates that the curing process is effective.

In fact, the polymeric chains are converted into a three-dimensional framework as has been already discussed. The release of oligomers is more difficult and even impossible for the EB cured fibres, since the cross-linking is almost totally achieved (no more Si–H bonds are observed on the IR spectra (Fig. 2)). For the oxygen-cured fibres, the slight weight loss might be due to insufficient cross-linking (which would induce an evolution of oligomers) or to an evolution of H_2O from the precursor, resulting from the oxidation of Si–H bonds according to the reaction:

$$2\text{Si–H} + O_2 \rightarrow \text{Si–O–Si} + H_2O$$

5.3.2. For $450 < T_p < 950$ °C

A second weight loss is observed beyond ≈500 °C for the uncured PCS which is assigned to the organic–inorganic transformation which has been reported previously by several authors [39, 30, 31, 33]. For the EB-cured fibres, no weight loss is observed until $T_p \approx 550$ °C (the ceramic yield at 950 °C being 84%). At the beginning of the conversion process a thermal cross-linking is thought to occur which would correspond to the weight loss observed in the 480–550 °C temperature range. The occurrence of this thermal postcuring is supported by the IR absorption spectra recorded for the uncured PCS pyrolysed at 600 °C (Fig. 4.).

The decrease of the intensity of both the ν(Si–H) and the δ(Si–CH_3) bands (respectively at 2100 and 1250 cm^{-1}) and the intensity increase of the Si–CH_2–Si bands (δ(CH_2) at 1355 cm^{-1} and ω(CH_2) at 1040 cm^{-1}) correspond to the condensation of PCS chains with dehydrogenation, according to the following equation:

$$\text{Si–CH}_3 + \text{Si–H} \rightarrow \text{Si–CH}_2\text{–Si} + H_2$$

Conversely, during this stage (up to ≈550 °C) no weight loss is observed for the cured fibres. Such a condensation mechanism is not expected to occur, since the cross-linking was almost fully achieved during the EB treatment.

At higher temperatures (i.e., for $500 < T_p < 950$ °C), the thermal decomposition of the side chains takes place: the remaining Si–H and Si–CH_3 bonds are broken in addition to the C–H bonds of the Si–CH_2–Si polymeric chains. An evolution of hydrogen and hydrocarbon gas (mainly methane) is thus observed. During this step no difference is expected between the uncured and EB-cured filaments, since the cross-linking process is thought to be fully achieved, by thermal curing for the former and EB curing for the latter. Indeed, the gas emission during the pyrolysis is actually very similar for both materials. Firstly, a methane evolution is detected from 450–500 °C with a maximum at 650 °C which is due to the rupture of Si–CH_3 bonds. Secondly, an evolution of hydrogen is also observed from 500–550 °C with a maximum at 700 °C, corresponding to the scission of the C–H bonds.

At $T_p = 900$ °C, the absorption band due to Si–CH_2–Si has almost vanished and a new peak appears at 815 cm^{-1}, which is assigned to Si–C bonds in silicon carbide (Fig. 4). A hydrogen formation is still detected for $T_p = 850$ °C, though the conversion of the PCS into an inorganic solid is nearly fully achieved. The pyrolytic material is amorphous at the end of the organometallic/mineral transformation of the PCS. Its chemical formula is almost the same whether or not the PCS filaments have been EB-cured, indicating that the curing and the pyrolysis were achieved under low oxygen concentrations and the EB-curing has no effect on the C:Si atomic ratio in the resulting ceramic material. The chemical analyses (Tables III and IV) show that the pyrolytic residue consist mainly of SiC, free carbon and trace amounts of silicon oxycarbide SiO_xC_y. Furthermore, it is thought that it also contains a small amount of hydrogen up to 1200 °C which is bonded to the free carbon atoms, a point which has been established by other authors [34, 35].

5.4. Thermal stability of the fibres

5.4.1. Thermal behaviour of the fibres under an inert atmosphere

5.4.1.1. Chemical changes. The chemical composition of the core of the filaments does not vary significantly for T_p values ranging between 900–1600 °C under argon and to 1750 °C under nitrogen (Table IV). However, some residual hydrogen is thought to be released and is responsible for a small diameter shrinkage and an increase of the density of the filaments. The high thermal stability of the core of the Si–C fibres, with respect to their oxygen-cured counterparts (as assessed by the TGA analyses) is related to the absence of significant amounts of the oxycarbide phase (observed to occur with an evolution of SiO and CO beyond ≈1100 °C, for the Si–C–O fibres) [21].

The fibre consists mainly (i.e., neglecting the small amount of silicon oxycarbide) of a mixture of SiC and

free carbon. From the Si–C phase diagram, it is expected to be chemically stable up to the decomposition temperature of SiC (reported to occur at $\approx 2500\,^{\circ}C$). However, the fact that it still contains ≈ 2.3 at % of oxygen (as SiO_xC_y) should result in some SiO and CO gas evolution at high temperature.

The concentration profiles, recorded from the surface of the fibre along a radial direction, shows that a thin carbon layer appears beyond pyrolysis temperatures of 1400 °C and keeps on growing as the temperature and the annealing time are raised, whatever the nature of the atmosphere (Fig. 7). This layer is thought to result from the decomposition of the SiC nanocrystals near the surface (although the decomposition of bulk SiC is reported to occur at a much higher temperature) and/or an active oxidation phenomenon of silicon carbide, due to residual oxygen in the atmosphere. The silicon monoxide is condensed on the cool parts of the furnace. It gives a mixture of Si and SiO_2 or reacts with the graphite crucible according to the following equation:

$$SiO_{(g)} + 2C_{(s)} \rightarrow SiC_{(s)} + CO_{(g)}$$

Thus silicon monoxide would not reach its equilibrium pressure in the gas phase.

When annealed under nitrogen at a pyrolysis temperature of 1600 °C, the AES profile shows a small amount of nitrogen in a 100 nm thick zone near the fibre surface, in addition to the carbon layer previously mentioned. These features correlate with the occurrence of nitridization of the fibre at high temperatures as has already been reported for Si–C–O fibres treated under a high nitrogen pressure [49].

5.4.1.2. Microstructural changes. The fibres resulting from the pyrolysis of the EB-cured PCS fibres remain amorphous up to about 1000 °C whatever the nature of the atmosphere. For a pyrolysis temperature of 1200 °C, the Debye-Scherrer pattern exhibits three broad peaks, corresponding to β-SiC showing that the amorphous material is undergoing crystallization. The SiC crystal size, as measured from TEM dark field images or calculated from the Scherrer equation is equal to about 2–3 nm. As previously mentioned, the fibre also contains free carbon. In the fibres containing a high oxygen concentration, free carbon was present as isolated BSU in the amorphous silicon oxycarbide phase [17, 18, 37]. Conversely, in the present EB-cured fibres, because of the very low amount of the SiO_xC_y phase, free carbon is present between the SiC crystals as wrinkled aromatic layers. When heat treated at higher temperatures, ($T_p = 1400$ and 1600 °C) it clearly appears that the thermal stability of the fibre microstructure is much higher in terms of grain growth rate of the SiC nanocrystals and organization state of the carbon phase. Thus as T_p is raised, the SiC grains slowly grow to a mean size of 6–8 nm at $T_p = 1600\,^{\circ}C$ ($t_p = 15$ min.) and 10 nm at $T_p = 1750\,^{\circ}C$ ($t_p = 1$ h). By comparison, under similar conditions, the Si–C–O fibres are totally decomposed with SiC crystals as large as several μm.

5.5. Mechanical behaviour

5.5.1. At room temperature

As shown in Fig. 13 the ambient temperature mechanical properties of the fibres depend on the temperature (T_p) at which they have been prepared, their oxygen content and the nature of the pyrolysis atmosphere (Ar or N_2).

The Young's modulus E and the failure strength σ^R initially increase as T_p is raised from 850 and 1200 °C for the O_2-cured fibres and up to 1400 °C for the EB-cured fibres. These features correlate with the increase of density associated to the evolution of hydrogen.

Conversely, beyond 1200 °C, the amorphous silicon oxycarbide phase is no longer stable. It decomposes with an evolution of CO and SiO, yielding a porous Si–C residue. As a result, a large decrease of both E and σ^R is observed for the O_2-cured fibres. The EB/O_2-fibre (oxygen content: 9 at %) is slightly more heat-resistant than the O_2-cured fibre. The oxycarbide phase is probably not present in a sufficient amount in that fibre to induce a drop in the mechanical properties at $T_p = 1400\,^{\circ}C$. Nevertheless, σ^R is almost nil when the fibres are treated at 1600 °C under oxygen. These features suggest that a 9 at % oxygen concentration is too large to preserve the fibre microstructure for $T_p > 1400\,^{\circ}C$.

The stiffness at ambient of the EB-cured fibres increases as T_p is raised to $\approx 1400\,^{\circ}C$ and slowly decreases beyond this value. The Young's modulus is high as compared to the Si–C–O fibres ($E = 250$ GPa instead of 130 GPa for $T_p = 1400\,^{\circ}C$) and correlates with the facts that; (i) the fibre is richer in crystalline SiC phase (a stiff phase) than its oxygen-cured counter part and (ii) there is almost no SiO_xC_y phase (a compliant phase) in the fibre. In a similar manner, the failure strength at ambient increases as T_p is raised and is still high at 1400 °C.

Despite the small amount of oxygen, a decomposition takes place at the fibre surface, resulting in the evolution of volatile products (assumed to be CO and SiO) and the formation of a silicon-depleted layer. This layer is thought to induce the formation of external flaws explaining the decrease of σ^R.

When the fibres are annealed under a nitrogen atmosphere, the tensile strength does not decrease until $T_p = 1600\,^{\circ}C$. This feature might correlate with the occurrence of nitridization at high temperatures. Jaskowiack showed in a similar manner that thermal treatment of Si–C–O fibres at 1600 °C in high pressures of N_2 are more effective in reducing weight loss, crystal growth with less strength loss than a similar treatment under pressures of argon [49]. A possible explanation is the formation of a protective SiCN(O) phase at the surface of the fibres. This nitridized layer may then seal off surface porosity and further reduce decomposition thus resulting in a greater strength retention.

The surface decomposition and the β-SiC grain growth are thought to be responsible for the tensile strength decrease observed for $T_p = 1750\,^{\circ}C$. However, the strength retention is still much higher than

for the Si–C–O fibres which are completely decomposed beyond 1500–1600 °C.

5.5.2. At high temperature

5.5.2.1. Creep tests. The relationships between the creep behaviour and the microstructure of the fibre are difficult to quantify, especially when a complex change in microstructure takes place during the creep test [50]. Nevertheless, the creep of the fibre exhibits two main features:

(i) The creep rate of the Si–C–O fibre is considerably higher than for the EB-cured fibre. This difference in creep behaviour can be assigned to their different microstructures. The EB-cured fibre only contains well crystallized SiC and free carbon phases (which are creep resistant, even at high temperature) whereas the Si–C–O fibre mainly consists of the amorphous SiO_xC_y phase which is thought to be very compliant and highly sensitive to creep at high temperatures.

(ii) The EB-cured fibre is also more creep resistant in terms of time to failure than its oxygen-cured counterpart. It is obvious that under the test conditions (1300 °C; argon), the microstructure of the Si–C–O fibre is unstable, resulting in a weight loss, a SiC grain growth and thus, a decrease in its mechanical properties. On the other hand, after an annealing treatment at 1400 °C under argon, the EB-cured fibre is stable at the creep test temperature from both a chemical and a microstructural point of view.

5.5.2.2. Tensile tests. Mechanical tests performed at high temperatures in air, combine three distinct effects: (i) the physical and mechanical properties (stiffness decrease, thermal expansion, creep, …), (ii) the effect of the thermal stability of the fibres (microstructure and chemical changes) and (iii) the effect of oxidation resistance. The results of the short term tensile tests in air (Fig. 15) suggest that the effect of oxidation (except near the surface) as well as that of thermal degradation, which are expected to be time dependent, are not very pronounced under the test conditions.

The tensile strength of the EB-cured filaments (annealed 15 min at 1600 °C under nitrogen) remains constant up to 1400 °C whereas that of standard Nicalon fibres decreases regularly from ambient to 1400 °C.

As already mentioned for the creep tests, a possible explanation for this behaviour are microstructural differences between the two fibres. However, at 1200 °C the strength of the two fibres are similar owing to the higher strength of the Nicalon fibre at ambient.

5.6. Electrical conductivity

The electrical conductivity (σ) dramatically increases when T_p is raised from 1000 to 1200 °C and then more slowly for $1200 < T_p < 1600$ °C. Furthermore, the electrical behaviour of the fibres is that of a semiconducting material, except for the highest T_p values where it tends towards that of a semi-metal (e.g., the electrical conductivity becomes high and almost independent of the measurement temperature for $T_p = 1600$ °C).

These features suggest that two conduction mechanisms are successively in operation as T_p is raised (for $1000 < T_p < 1200$ °C and $1200 < T_p < 1600$ °C) that are dependant on the fibre microstructure.

On the basis of the evolution of the fibre microstructure with T_p, the electrical behaviour can be discussed as follows:

5.6.1. For $1000 < T_p < 1200$ °C

For $T_p = 1000$ °C, the low electrical conductivity and the semi-conducting behaviour of the fibre might be related to the rather poor crystallization state of the free carbon as well as the possible presence of residual hydrogen [34, 35]. When T_p is raised to 1200 °C, both an evolution of hydrogen and an organization of the free carbon occurs with consequently a fast increase of σ at a given measuring temperature and a decrease of the activation energy. Such features have also been reported for coals [40, 51].

5.6.2. For $1200 < T_p < 1600$ °C

The change observed in the conductivity and its temperature dependence are obviously related to the microstructural change, i.e., the growth of the β-SiC nanocrystals and the organization of the carbon phase. The increase in size of the carbon layer stacks and the formation of a continuous network ordering might give rise to a percolation effect.

The carbon-rich layer observed on the fibres pyrolysed at $T_p = 1600$ °C has no significant effect on the electrical behaviour, since the removal of this layer by oxidation neither changes markedly the conductivity level nor the activation energy. The carbon resulting from the fibre surface degradation may not be dense and/or organized enough to play a significant part in the electrical behaviour of the fibre.

5.7. Oxidation in dry oxygen

The oxidation of Si-based materials including SiC has been studied by many authors [9–11, 41–47]. The high oxidation resistance is due to the formation of a protective silica layer which limits further oxidation. The kinetics of the growth of the oxide layer obey a parabolic law suggesting that the oxidation is controlled by a diffusion phenomenon. This mechanism involves the transport of molecular oxygen by permeation across the growing oxide film [41]. The activation energies range from 80–500 kJ mol^{-1} the dispersion being related to the nature of the materials (powders, single crystals, polycrystalline materials such as CVD, sintered SiC).

Warren and Anderson [44], Clark *et al.* [45] and more recently Filipuzzi and Naslain [46] have investigated the oxidation of oxygen-cured Nicalon NL202 fibres in air or dry oxygen by TGA. For 800 °C $< T <$ 1200 °C passive oxidation takes place with the formation of amorphous or crystallized SiO_2.

Furthermore, the activation energy values are lower (70–80 kJ) for the Si–C–O fibres than those reported for pure SiC. A possible explanation could be the presence of hydrogen in the silica (coming from the bulk of the fibre) and/or micropores in the oxide film. Above 1200 °C, the kinetics of oxidation of the fibres no longer obey a parabolic law due to the thermal metastability of the SiO_xC_y phase.

The microstructure and the chemical composition of the Si–C fibre studied in the present work are different: on the one hand, the oxygen content is much lower and does not contribute significantly to the formation of silica, but on the other hand, a free carbon phase surrounds β-SiC nanocrystals, whereas in the Si–O–C fibre, discrete carbon BSU are dispersed within the oxycarbide phase. Thus, the free carbon might be much more accessible to oxygen which might lead to the formation of a non-protective oxide layer which possibly, could dramatically enhance the oxidation kinetics.

In the oxidation mechanism of the fibre, two opposite gas fluxes diffuse through the silica layer: (i) the oxygen flux from the outer surface to the fibre/oxide interface and (ii) the carbon oxides flux (CO or/and CO_2) in the opposite direction. Furthermore, hydrogen is present in very small amounts (the fibres were heat-treated at 1400 °C before the oxidation tests) which may lead to limited H_2 or H_2O fluxes through the oxide layer. As previously mentioned, molecular oxygen permeation through the growing silica is thought to be the controlling mechanism in the oxidation of the fibre. The diffusion of the carbon oxide species as a rate controlling step has been ruled out since Zheng *et al.* showed that such molecules diffuse readily through silica [52]. Furthermore, water vapour in small amounts is known to enhance SiC oxidation [53]. It seems unlikely that the diffusion of H_2/H_2O species produced from residual hydrogen in the fibre may control the oxidation of the fibres. The hydrogen concentration within the fibre is thought to be too low to play an important part in the oxidation of the filaments.

The morphology of the silica layer is also an important parameter in the oxidation kinetics. The surface of the oxide film remains smooth and crack-free whatever the testing temperature (Fig. 22). The thickness of the silica is constant along the periphery of the fibre showing that the oxidation was not locally favoured by flaws (bubbles, microcracks within the silica layer) or by any inhomogeneity in the chemical composition of the fibre which would have favoured the oxygen diffusion and thus, the oxidation.

A crystallization of the oxide layer is also observed. The silica formed at 1000 °C is totally amorphous. It starts to crystallize beyond 1200 °C and mainly consists of α-cristobalite at 1400 °C. This phenomenon apparently does not lead to any damage in the oxide film (as observed by SEM) despite the occurrence of a volume change and a viscosity loss during the glass–cristobalite transformation.

Furthermore, the growth of the silica also leads to an increase of the oxidized filament volume. The ratio of product to reactant volumes (Δ) is equal to 1.58. When $\Delta > 1$ the oxide layer has the capability to cover the substrate in a continuous manner but a high Δ value would induce mechanical stresses and thus form cracks within the silica or at the oxide/substrate interface. Such a phenomenon has not been observed. The crystallized silica layer is thought to be viscous enough at high temperatures, to release the mechanical stresses and thus, to cover the ceramic in a continuous manner even at 1400 °C, for low thickness values ($e < 1$ μm).

On the basis of the previous discussion, the oxidation kinetics data can be discussed as follows.

As shown in section 3, the kinetics of growth (k_T) of the silica layer on EB-cured filaments in dry oxygen obey a parabolic law in the temperature range 1000–1400 °C for $e \leqslant 0.7$ μm. The parabolic rate constant values are very similar to those obtained for the oxygen-cured fibre within the range 1000–1200 °C. Nevertheless, in the present study, the k_T value is observed to be slightly higher than that for the Si–C–O fibre for $T < 1200$ °C. On the other hand, the parabolic growth law is still obeyed up to 1400 °C for the EB-cured fibre whereas it is no longer valid beyond 1200 °C for the Si–C–O Nicalon fibre [46]. This feature is probably related to the higher thermal stability of the EB-cured fibres. The well known decomposition/crystallization process occurring for the high oxygen content fibres may influence the oxidation kinetics. As an example, the thickness of the silica formed at 1400 °C for $t = 7$ h is significantly lower for the EB-cured fibre than that for the Si–C–O fibre for $t = 10$ h (0.65 μm versus 3 μm). The complex degradation which takes place in the latter is thought to enhance the oxygen diffusion through the oxide layer.

As already observed for various Si-based materials, the oxidation kinetics under dry oxygen are thermally activated as shown in an Arrhenius plot (Fig. 21). Furthermore, the variations of $\ln k_D$ versus $1/T$ are observed to be linear within the whole temperature range studied. The value of the apparent activation energy is 96 $kJ \cdot mol^{-1}$ which is similar to that for the Si–C–O fibres (90 $kJ \cdot mol^{-1}$) [46] and, slightly lower than that reported for pure silicon (119 kJ [41]).

This similarity of the activation energies strongly suggests that the oxidation of the EB-cured fibres within the temperature range 1000–1400°C is controlled by the same mechanism as for SiC or silicon which is the permeation of molecular oxygen across the growing oxide film. In fact, the activation energy reported for the diffusivity of oxygen through fused silica is 113 $kJ \cdot mol^{-1}$ [54]. Nevertheless, k_T values are higher at a given temperature and E_a values are much lower for SiC fibres than those previously reported for pure polycrystalline SiC (150–300 $kJ\,mol^{-1}$). The oxidation of such materials is complicated when compared to that of single-crystal or pure silicon because of the presence of sintering aids and the propensity for crystallization of the oxide film. Costello and Tressler reported E_a values as low as 120 $kJ\,mol^{-1}$ for the oxidation of the (0 0 0 1) Si face in a SiC single crystal and 140 $kJ\,mol^{-1}$ for thermally deposited SiC (CNTD) [43]. This oxidation behaviour is similar to that observed for the SiC based-fibres and might be

related to the low level of impurities present in the material if we neglect the oxygen free carbon.

6. Conclusion

Model SiC-based fibres with a low oxygen content (2–3 at %) have been prepared by means of an irradiation curing process.

The curing mechanism involves the formation and condensation of free radicals leading to Si–CH_2–Si and to a lesser extent Si–Si and C–C bridges between polymeric chains and to an evolution of hydrogen. A significant weight loss is observed during the pyrolysis of the cured-fibres corresponding to the organic–mineral transformation with a gas evolution (mainly H_2 and CH_4). The ceramic yield of the cured-fibres is much higher than that for the uncured PCS (84% versus 56%) since no oligomer evolution occurs after cross-linking caused by irradiation. The chemical composition of the resulting ceramic fibres is close to that of PCS pyrolytic residues.

Ceramic fibres prepared from PCS according to a spinning-curing-pyrolysis procedure exhibit much better properties at high temperatures when the oxygen-curing step is replaced by an EB-curing under an inert atmosphere. The fibres which only contain a small amount of SiO_xC_y, are chemically stable at high temperatures under an inert atmosphere (with no significant weight loss and gas evolution). They consist of a mixture of SiC (about 5 nm size) and free carbon. This carbon is present as turbostratic stacks of wrinkled layers and is better organized than that in oxygen-cured fibres. Its presence between the SiC nanocrystals is thought to be responsible for the relatively good thermal stability of the microstructure (the carbon phase at the SiC grain boundary preventing an excessive crystal growth).

The SiC fibres exhibit better mechanical properties than their Si–O–C counterparts in terms of tensile strength at ambient after annealing but also at high temperatures in terms of tensile strength and creep resistance.

Owing to their improved thermal stability, the oxidation parabolic kinetic law is still obeyed up to 1400 °C (in other words the silica layer is still protective), whereas this is no longer true for the Si–C–O fibre beyond 1200 °C.

Acknowledgements

This work has been supported through a grant given by CNRS and SEP. The authors thank R. Bodet for his assistance in the creep tests.

References

1. D. J. JOHNSON, in "Introduction to carbon science", edited by H. Marsh (Butterworths, London, 1989) p. 197.
2. M. S. DRESSELHAUS, G. DRESSELHAUS, K. SUGIHARA, I. L. SPAIN and H. A. GOLBERG, in "Graphite Fibres and Filaments", edited by M. Cardona (Springer Verlag, London, 1988) p. 230.
3. F. LAMOUROUX, X. BOURRAT, R. NASLAIN and J. SEVELY, *Carbon* **31**(8) (1993) 1273.
4. A. K. DHINGRA, *Phil. Trans. R. Soc. London* **A294** (1980) 411.
5. D. B. MARSHALL, F. F. LANGE and P. D. MORGAN, *J. Amer Ceram. Soc.* **70** (1987) C187.
6. D. J. PYSHER, K. C. GORETTA, R. S. HODDER Jr and R. E. TRESSLER, *ibid* **72** (1989) 284.
7. D. J. PYSHER and R. E. TRESSLER, *J. Mater. Sci.* **27** (1992) 428.
8. G. S. CORMAN, *Ceram. Engng. Sci. Proc.* **12** (1991) 1745.
9. G. ERVIN, *J. Amer. Ceram. Soc.* **41** (1958) 347.
10. P. J. JORGENSEN, M. E. WADSWORTH and I. B. CUTLER *ibid.* **42** (1959) 613.
11. S. C. SINGHAL, *J. Mater. Sci* **11** (1976) 1246.
12. J. A. DI CARLO, *ibid.* **21** (1986) 217.
13. E. LARA-CURZIO and S. S. STERNSTEIN, *Comp. Sci. & Tech.* **46** (1993) 265.
14. S. YAJIMA, J. HAYASHI and M. OMORI *Chem. Lett.* **9** (1975) 931.
15. S. YAJIMA, K. OKAMURA and J. HAYASHI, *ibid.* **12** (1975) 1209.
16. T. YAMAMURA, T. ISHIRKAWA, M. SHIBUYA and T. ISHIKAWA, *J. Mater. Sci.* **23** (1988) 2589.
17. C. LAFFON, A. M. FLANCK, P. LAGARDE, M. LARIDJANI, R. HAGEGE, P. OLRY, J. COTTERET, J. DIXMIER, J. L. MIQUEL, H. HAMMEL and A. P. LEGRAND, *ibid.* **24** (1989) 1503.
18. L. PORTE and A. SARTRE, *ibid.* **24** (1989) 271.
19. T. MAH, N. LECHT, D. E. Mc CULLUM, J. R. HOENIGMAN, H. M. KIM, A. P. KATZ and H. A. LIPSITT *ibid.* **19** (1984) 1119.
20. T. J. CLARK, R. M. ARONS, I. B. STAMATOFF and J. RABE, *Ceram. Engng. Sci. Proc.* **6** (1985) 576.
21. S. M. JOHNSON, R. D. BRITTAIN, R. H. LAMOREAUX and D. J. ROWCLIFFE, *J. Amer. Ceram. Soc.* **71** (1988) C132.
22. T. SHIMOO, H. CHEN and K. OKAMURA, *J. Ceram. Soc. Jpn* **100** (1991) 48.
23. T. J. CLARK, M. JAFFE, J. R. and N. R. LANGLEY, *Ceram. Engng. and Sci. Proc.* **7** (1986) 901.
24. M. H. JASKOWIAK and J. A. DI CARLO, *J. Amer. Ceram. Soc.* **72** (1989) 192.
25. B. A. BENDER, J. S. WALLACE and D. J. SCHRODT, *J. Mater. Sci.* **26** (1991) 970.
26. K. OKAMURA, M. SATO, T. SEGUSHI and S. KAWANISHI, in "Controlled Interphases in Composite Materials" edited by H. Ishida (Elsevier, New York, 1990) p. 209.
27. M. TAKEDA, Y. IMAI, H. ICHIKAWA, T. ICHIKAWA, T. SEGUSHI and K. OKAMURA, *Ceram. Engng. Sci. Proc.* **12** (1991) 1007.
28. J. F. VILLENEUVE, D. MOCAER, R. PAILLER, R. NASLAIN and P. OLRY, *J. Mater. Sci.* **28** (1993) 1227.
29. R. BODET, PhD thesis n°986, University of Bordeaux (1993).
30. Y. HASEGAWA, M. IIMURA and S. YAJIMA, *J. Mater. Sci.* **15** (1980) 720.
31. Y. HASEGAWA and O. OKAMURA, *ibid.* **18** (1983) 3633.
32. *Idem*, *ibid.* **21** (1986) 321.
33. Y. HASEGAWA, *ibid.* **24** (1989) 1177.
34. C. GERARDIN, PhD thesis, University of Paris VI, 1991.
35. C. GERARDIN, M. HENRY and F. TAUTELLE, *Mat. Res. Soc. Symp. Proc.* **271** (1992) 777.
36. Y. SAZAKI, Y. NASHINA, M. SATO and K. OKAMURA, *J. Mater. Sci.* **22** (1987) 443.
37. P. LE COUSTUMER, M. MONTHIOUX and A. OBERLIN, *J. Eur. Ceram. Soc.* **11** (1993) 95.
38. E. BOUILLON, D. MOCAER, J. F. VILLENEUVE, R. PAILLER, R. NASLAIN, M. MONTHIOUX, A. OBERLIN, C. GUIMON and G. PFISTER-GUILLOUZO, *J. Mater. Sci.* **26** (1991) 1517.
39. E. BOUILLON, F. LANGLAIS, R. PAILLER, R. NASLAIN, J. C. SARTHOU, A. DELPUECH, C. LAFFON, P. LAGARDE, F. CRUEGE, P. V. HUONG, M. MONTHIOUX and A. OBERLIN, *ibid.* **26** (1991) 1333.
40. F. CARMONA, P. DELHAES, G. KERYER and J. P. MANCEAU, *Solid State Comm.* **14** (1974) 1183.

41. B. E. DEAL and A. S. GROVE, *J. Appl. Phys.* **36** (1965) 3770.
42. J. A. COSTELLO and R. E. TRESSLER, *J. Amer. Ceram. Soc.* **64** (1981) 327.
43. *Idem*, *ibid.* **69** (1986) 674.
44. R. WARREN and C. H. ANDERSON, *Composites* **15** (1984) 101.
45. T. J. CLARK, E. R. PRACK, M. I. AIDER and L. C. SAWYER, *Ceram. Engng. Sci. Proc.* **7** (1986) 901.
46. L. FILIPUZZI and R. NASLAIN, in Proceeding of the 7th CIMTEC, Mater. Sci. Monograph 68 Adv. Structural Inorg. Composites, edited by P. Vincenini (Elsevier, Amsterdam, 1991) p. 35.
47. D. MOCAER, G. CHOLLON, R. PAILLER, L. FILIPUZZI and R. NASLAIN, *J. Mater. Sci.* **28** (1993) 3059.
48. K. OKAMURA, T. MATSUKAWA and Y. HASEGAWA, *J. Mater. Sci. Lett.* **4** (1985) 55.
49. M. H. JASKOWIAK, NASA Technical Memorandum 103245 (1991).
50. N. JIA, R. BODET and R. E. TRESSLER, *J. Amer. Ceram. Soc.* **76** (1993) 3051.
51. M. RICCI, PhD thesis n°644, University of Bordeaux (1991).
52. K. E. SPEAR, R. E. TRESSLER, Z. ZHENG and H. DU, *Ceramic Trans* **10** (1990) 1–18.
53. E. J. OPILA, *J. Amer. Ceram. Soc.* **77** (1994) 730.
54. F. J. NORTON, *Nature* **171** (1961) 701.

Received 19 April
and accepted 21 May 1996